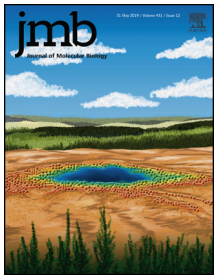

The Tumor Suppressor ING5 Is a Dimeric, Bivalent Recognition Molecule of the Histone H3K4me3 Mark

Georgina Ormaza[1,†], Jhon A. Rodríguez[1,†], Alain Ibáñez de Opakua[1], Nekane Merino[1], Maider Villate[1], Irantzu Gorroño[1], Miriam Rábano[1], Ignacio Palmero[2], Marta Vilaseca[3], Robert Kypta[1,4], María d.M. Vivanco[1], Adriana L. Rojas[1] and Francisco J. Blanco[1,5]

*1 - **CIC bioGUNE,** Parque Tecnológico de Bizkaia, 48160 Derio, Spain*
*2 - **Instituto de Investigaciones Biomédicas "Alberto Sols",** CSIC-UAM, 28029 Madrid, Spain*
*3 - **Institute for Research in Biomedicine,** 08028 Barcelona, Spain*
*4 - **Department of Surgery and Cancer,** Imperial College London, London, W12 0NN, UK*
*5 - **IKERBASQUE,** Basque Foundation for Science, 48011 Bilbao, Spain*

***Correspondence to Francisco J. Blanco:** CIC bioGUNE, Parque Tecnológico de Bizkaia, 48160 Derio, Spain.*
fblanco@cicbiogune.es
https://doi.org/10.1016/j.jmb.2019.04.018
Edited by M. Guss

Abstract

The INhibitor of Growth (ING) family of tumor suppressors regulates the transcriptional state of chromatin by recruiting remodeling complexes to sites with histone H3 trimethylated at lysine 4 (H3K4me3). This modification is recognized by the plant homeodomain (PHD) present at the C-terminus of the five ING proteins. ING5 facilitates histone H3 acetylation by the HBO1 complex, and also H4 acetylation by the MOZ/MORF complex. We show that ING5 forms homodimers through its N-terminal domain, which folds independently into an elongated coiled-coil structure. The central region of ING5, which contains the nuclear localization sequence, is flexible and disordered, but it binds dsDNA with micromolar affinity. NMR analysis of the full-length protein reveals that the two PHD fingers of the dimer are chemically equivalent and independent of the rest of the molecule, and they bind H3K4me3 in the same way as the isolated PHD. We have observed that ING5 can form heterodimers with the highly homologous ING4, and that two of three primary tumor-associated mutants in the N-terminal domain strongly destabilize the coiled-coil structure. They also affect cell proliferation and cell cycle phase distribution, suggesting a driver role in cancer progression.

Introduction

In eukaryotic cells, nuclear DNA is packed with proteins into chromatin. The nucleosome is the fundamental unit of chromatin, with two superhelical turns of DNA wound around an octamer of the four core histones. The flexible N-terminal tails of the histones are rich in positive charges which pair up with the negatively charged DNA phosphate backbone, allowing for high levels of chromatin compaction [1]. The structure of chromatin is highly dynamic and crucially supports DNA replication, repair, and transcription [2,3]. Its regulation is largely based on post-translational covalent modifications of certain residues at the N-terminal histone regions, which directly affect the level of chromatin condensation and/or recruit to their location specific chromatin remodeling complexes. Histone tails are selectively modified by enzymatic complexes containing proteins with domains that recognize one or more of the possible histone modifications [4].

The family of tumor suppressors INhibitors of Growth (ING) consists of five homologous proteins [8] that regulate the transcriptional state of chromatin by recruiting remodeling complexes to sites with histone H3 trimethylated at Lysine 4 (H3K4me3).

This histone post-translational modification is recognized by the C-terminal ING PHD [9]. ING1 and ING2 form part of histone deacetylase (HDAC) complexes, while ING3, 4, and 5 form part of histone acetyl transferase (HAT) complexes [10]. Sequences of the ING proteins (Fig. 1) show that they have a conserved N-terminal region, a central non-conserved region containing the NLS and a conserved C-terminal PHD [5]. Structures of the PHD fingers of ING1 [11], ING2 [12], ING4 [13] and ING5 [14] bound to H3K4me3 fragments have been determined, displaying broadly conserved features with some differences in the conformations of the bound H3K4me3 peptides [13]. The structural organization of full length ING4 has also been studied [15]. It is a dimer, with its Nt folded into an antiparallel homodimer with a coiled-coil structure [16], while the central region connecting the two folded domains is flexible and disordered. ING4 forms part of the HBO1 HAT complex [10], and promotes acetylation of H3 [17]. The ING4 paralog ING5 can also be part of HBO1, but only ING5 [10] forms part of the MOZ/MORF HAT complex, which also acetylates histone H3. The high homology between ING4 and ING5 suggests that they may form heterodimers [16], as has been found for other tumor suppressors [18]. We set out to experimentally study the structural organization of ING5. With this aim, the full-length ING5 protein, as well as fragments spanning the Nt, and the PHD finger have been produced and analyzed by NMR, x-ray diffraction, and other techniques. We show that ING5 dimerizes through its Nt with a coiled-coil structure and results in a molecule with two PHD fingers that independently bind to H3K4me3 histone marks. The two domains are connected by a very flexible central region that can bind dsDNA. Two of three mutants at the Nt described in primary tumors strongly destabilize the protein and affect cell proliferation and cell cycle phase distribution.

Results

ING5 is a dimer and a bivalent reader of the H3K4mark

To explore the domain organization of ING5, we defined domain boundaries analogous to those previously identified in ING4 [15]. Because of the high-sequence homology, structure predictions give similar results: the presence of a coiled coil with two long helices in the N-terminal conserved domain, a disordered non-conserved central region rich in positively charged amino acids that contains the nuclear localization sequence [5], hereafter named NLS, and three short β-strands in the C-terminal PHD finger. The high level of sequence identity at the N-terminus also suggests that ING5 will form dimers, as does ING4.

The molar mass of ING5 measured by SEC-MALS is 57 kDa (Fig. 2A), which is consistent with the calculated mass of a dimer (60 kDa). However, it elutes from the SEC column at a smaller volume than expected for a dimer, indicating that ING5 has an elongated shape and/or large regions that are flexible and disordered [19]. In both instances, it would elute at a smaller volume than a globular protein of the same mass. ING5 has a high content of helical structure, as indicated by the two minima at 209 and 223 nm and the positive ellipticity below 200 nm in its circular dichroism (CD) spectrum (Fig. 2B). The absolute ellipticity indicates, however, that a large part of the chain is not helical. The Nt domain is also a dimer (Fig. 2A), with a measured molar mass of 23 kDa (the calculated mass of a dimer is 25 kDa). Both ING5 and the Nt domain show cooperative thermal denaturation, although with different mid-point melting temperatures, indicating the presence of a defined tertiary fold for both proteins (Fig. 2C).

The NMR spectrum of the 60 kDa ING5 dimer is similar to that of ING4 [15] (for solubility reasons, they were acquired at pH 8.0 and 6.5, respectively). It shows a set of sharp and dispersed backbone amide resonances that correspond to the PHD finger (see below) and a set of resonances non-dispersed in the ^{1}H dimension (Fig. 3A). The observation of a single set of resonances for the two PHD fingers of the dimer indicates that they are chemically equivalent. Altogether these results suggest that the structural organization of ING5 is similar to that of ING4: an N-terminal dimeric coiled-coil domain and a C-terminal PHD connected by a flexible NLS segment, the three regions being structurally independent.

The crystal structure of the C-terminal PHD finger has been previously reported bound to an H3K4me3 peptide [14], and consists of the canonical PHD fold, with its characteristic C_4HC_3 zinc finger motif [13]. We have analyzed the structure of the PHD in solution and found that it is a monomeric protein (Fig. S1A) with a $^{1}H–^{15}N$ NMR spectrum (Fig. 3B) very similar to the set of dispersed signals in the spectrum of ING5 (Figs. 3A and S1B). A detailed analysis shows that for 83% of the backbone amide signals of the PHD, the ^{1}H and ^{15}N resonance frequencies closely match those of a corresponding signal in the spectrum of full-length ING5 (chemical shift deviations <0.065 ppm). This result demonstrates that the Nt and the PHD are independent non-interacting domains linked by a flexible NLS segment. Some of the PHD NMR signals exhibit chemical shift perturbations upon addition of H3K4me3 peptide, which mimic those observed with the full-length protein (Fig. 3). The fitting of the perturbations measured for those residues that shift the most yields dissociation constants of 7.0 ± 2.7 and 18.4 ± 2.8 μM at 25 °C for the full-length ING5 and the PHD finger, respectively (average and standard deviations; Fig. S2). These values are in the same low micromolar range as the

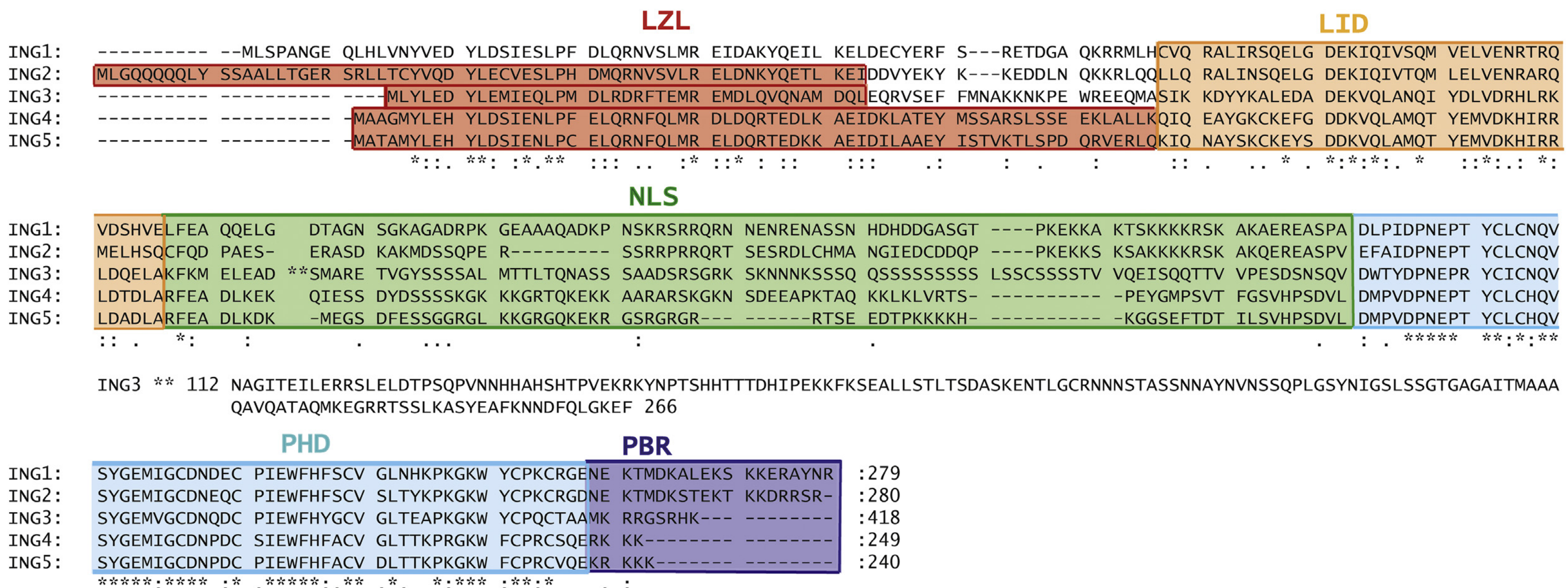

Fig. 1. Sequence alignment of the human ING proteins. Sequences can be generally divided into three regions [5], a conserved N-terminal domain (Nt; except for ING1) formed by leucine zipper like region (red) and lamin interaction domain (orange) [6], a non-conserved central region containing the nuclear localization signal (NLS; green), and a highly conserved C-terminal region, containing the plant homeodomain (PHD; cyan), followed by the PolyBasic Region (PBR; blue). For ING1, the most frequently observed p33ING1b splicing variant is used. For the rest the full amino acid sequence is used. The alignment was performed using ClustalW [7]. Asterisks indicate strict conservation, colons conserved amino acids, and dots conserved polar or apolar character. The two asterisks in ING3 indicate non-aligning sequence (residues 112-266).

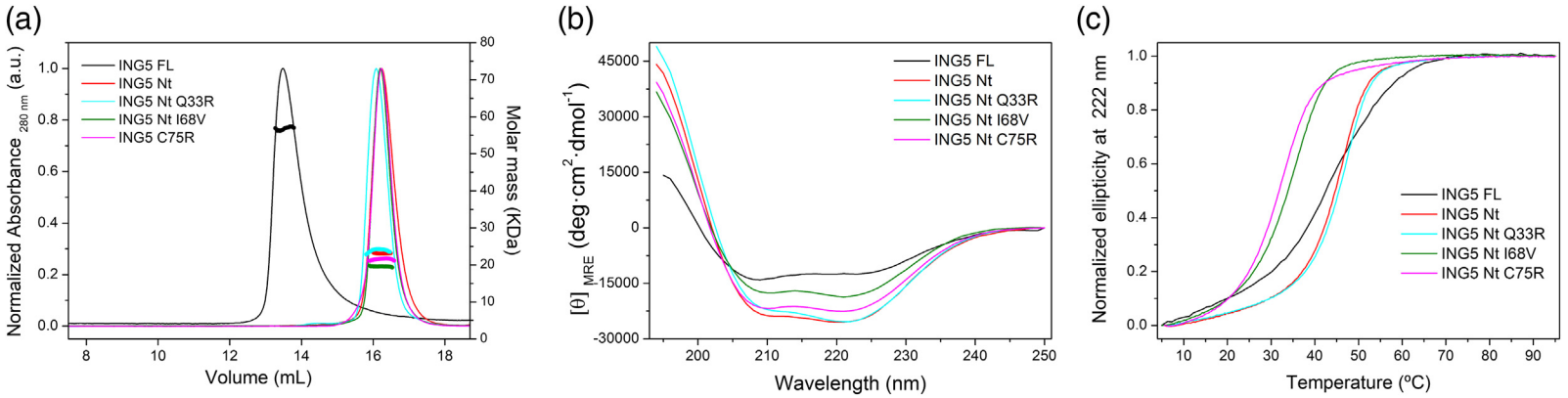

Fig. 2. ING5 dimerizes in solution through its N-terminal helical domain. (A) SEC-MALS analysis of ING5 (black), Nt (red), and its mutants (Q33R in cyan, I68V in olive, and C75R in magenta). These mutants are found in cancer and are described later in the main text. All data were obtained in 20 mM Tris (pH 8.0), 300 mM NaCl, 1 mM DTT, at 25 °C. The exclusion volume of the column is 8.7 mL. (B) CD spectra of ING5 molecules in the same conditions as in panel A. (C) Thermal denaturation of ING5 molecules in the same buffer as in panel A.

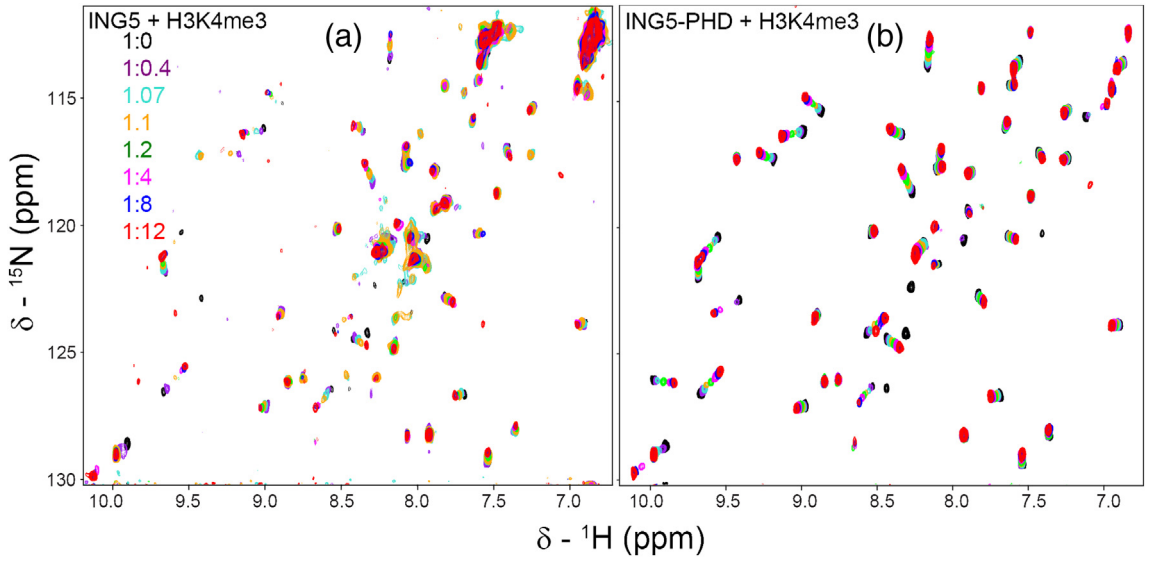

Fig. 3. ING5 binding to H3K4me3. (A) $^{1}H–^{15}N$ heteronuclear single quantum coherence spectroscopy (HSQC) NMR spectra of an 11 μM sample of ING5 at 25 °C in 20 mM Tris buffer (pH 8.0) 300 mM NaCl and 1 mM DTT in the presence of increasing amounts of histone H3K4me3 peptide. The spectra at intermediate molar ratios have been plotted with lower contour levels than the others to visualize the low intensity signals. (B) $^{1}H–^{15}N$ HSQC NMR spectra of ING5 PHD finger along the titration with H3K4me3 peptide in the same experimental conditions as the spectra shown in panel A.

measured for the isolated PHD of ING5 by fluorescence (2.4 ± 1.0 μM) and for the full-length and isolated PHD of ING4 by NMR at 25 °C (1.3 ± 1.0 and 3.9 ± 1.0 μM, respectively), considering the errors and the different buffer used for ING4 [20 mM sodium phosphate (pH 6.5), 50 mM NaCl, I mM DTT] [13,14]. The PHD finger of ING5 binds histone H3K4me3 with an affinity 2 orders of magnitude higher than to the unmethylated tail [14]

The Nt domain of ING5 forms a symmetric coiled-coil dimer

The helical pattern in the CD spectrum of the Nt domain of ING5 is more pronounced than that of the full-length protein, with an ellipticity ratio $[\Theta]_{222nm}/[\Theta]_{208nm} > 1$, typical of coiled-coil structures [20]. The limited solubility of ING5 (about 10 μM at pH 8.0, and decreasing with pH) prevents the observation of most

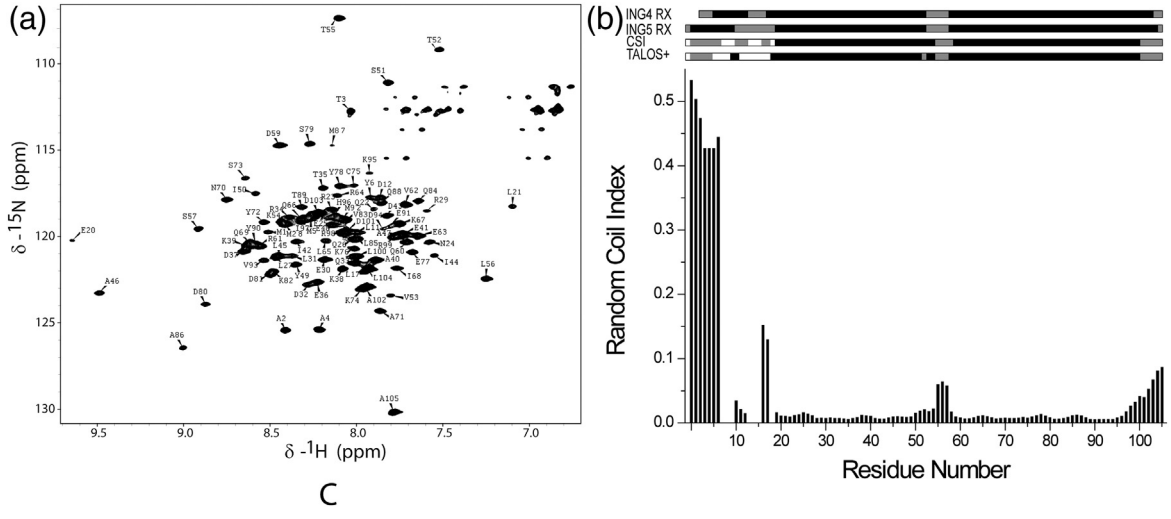

Fig. 4. Structural analysis of ING5 Nt in solution by NMR. (A) $^{1}H–^{15}N$ transverse optimized spectroscopy (TROSY) NMR spectrum of ING5 Nt at 25 °C in 50 mM Mops (pH 7.3), 1 mM DTT, and 300 mM NaCl. The unassigned signals in the upper-right corner of the figure correspond to Asn and Gln side chains. (B) Secondary structure of ING5 Nt from backbone resonances chemical shift analysis using different methods (helix in black, coil in gray and unknown in white). For comparison, the structure in the crystals of ING4 and ING5 Nt is also shown.

of the signals of the Nt domain in the NMR spectrum of the full-length protein, which are broader than the signals of the small PHD (as expected for a 28-kDa elongated coiled-coil domain). The higher solubility of the isolated Nt domain allows the observation of 93 signals in the $^{1}H–^{15}N$ correlation spectrum, which could be assigned to specific residues (Fig. 4A). Although there are 10 residues for which no amide signal was detected, the observation of a single set of resonances (only one signal is observed for each residue) indicates that the dimer is symmetric. About 92% of the CA resonances could also be assigned, but the limited sensitivity of the NMR experiments only allowed measurement of 41% and 17% of the HA and CB chemical shift values, respectively. Chemical shift analysis shows that there are two long helices spanning residues 18–54 and 58–100 (Fig. 4B). These results indicate that the structure is similar to the crystal structure of the Nt of ING4 [16], which forms a symmetric dimer and antiparallel coiled-coil fold based on two long helices named α2 (residues 17–52) and α3 (residues 58–103). The formation of a symmetric dimer structure of ING5 Nt is consistent with the observation of a single set of NMR signals and with the low sensitivity of the NMR experiments (because of its size, helical structure, and elongated shape), as occurred with the Nt domain of ING4 [15]. The presence of a short helical segment analogous to the N-terminal α1 helix of ING4 (residues 5–12) could not be confirmed in ING5 Nt in solution by NMR. The N-terminal 6 residues of ING5 are flexible and disordered as indicated by their chemical shifts, and for several of the following residues, no NMR signal was detected. In the crystal structure of ING4 Nt, this short helix (residues 5–12) was found to make contacts not within the dimer to which it belongs but with another dimer, suggesting that it could be a dynamic local structure stabilized by the crystal lattice. The NMR data on ING5 suggest that this segment may be involved in conformational exchange equilibria that cause some of the NMR signals to become non-detectable.

Crystallization trials of ING5 Nt yielded crystals (Fig. S3A) that after optimization were suitable for x-ray diffraction and data collection at 3.2-Å resolution (Fig. S3B). The structure was solved by molecular replacement using the crystal structure of the homologous ING4 Nt [16] and refined to R_{work} of 21.1% and R_{free} of 24.8%. A summary of the crystallographic data statistics is shown in Table 1.

Table 1. Crystallography data collection and refinement statistics.

	ING5-Nt	ING5-Nt
Construct	$ING5_{WT}$	$ING5_{C19S}$
Data collection		
Space group	$P6_522$	$P6_522$
Cell dimensions		
a, *b*, *c* (Å)	135.63, 135.63, 96.67,	140.94, 140.94, 92.32
α, *β*, *γ* (°)	90.0, 90.0, 120.0	90.0, 90.0, 120.0
Resolution (Å)	44.70 (3.39–3.20)	92.32 (3.27–3.10)
R_{merge}	0.08 (0.85)	0.17 (0.93)
$CC_{1/2}$	0.99 (0.70)	0.98 (0.87)
$I/\sigma(I)$	47.5 (6.2)	9.7 (3.1)
Completeness (%)	99.9 (99.9)	100 (100)
Redundancy	7.6 (3.5)	18.3 (18.8)
Refinement		
No. reflections	9076	10,275
R_{work}/R_{free}	21.10/24.80	21.53/25.38
No. atoms		
Protein	1767	1752
Ions/ligands	44[a]	6[b]
Water	13	3
B-factors (Å^2)		
Protein	104.68	99.43
Ions	142.76	81.22
Water	175.70	71.80
R.m.s deviations		
Bond lengths (Å)	0.009	0.007
Bond angles (°)	0.99	1.024
Ramachandran favored (%)	98.0	96.0
Ramachandran outliers (%)	0.0	0.0
PDB code	5ME8	5MTO

Values in parentheses correspond to the highest-resolution shell.
[a] Molecules of EDO and MPD.
[b] Sulfate and Na ions.

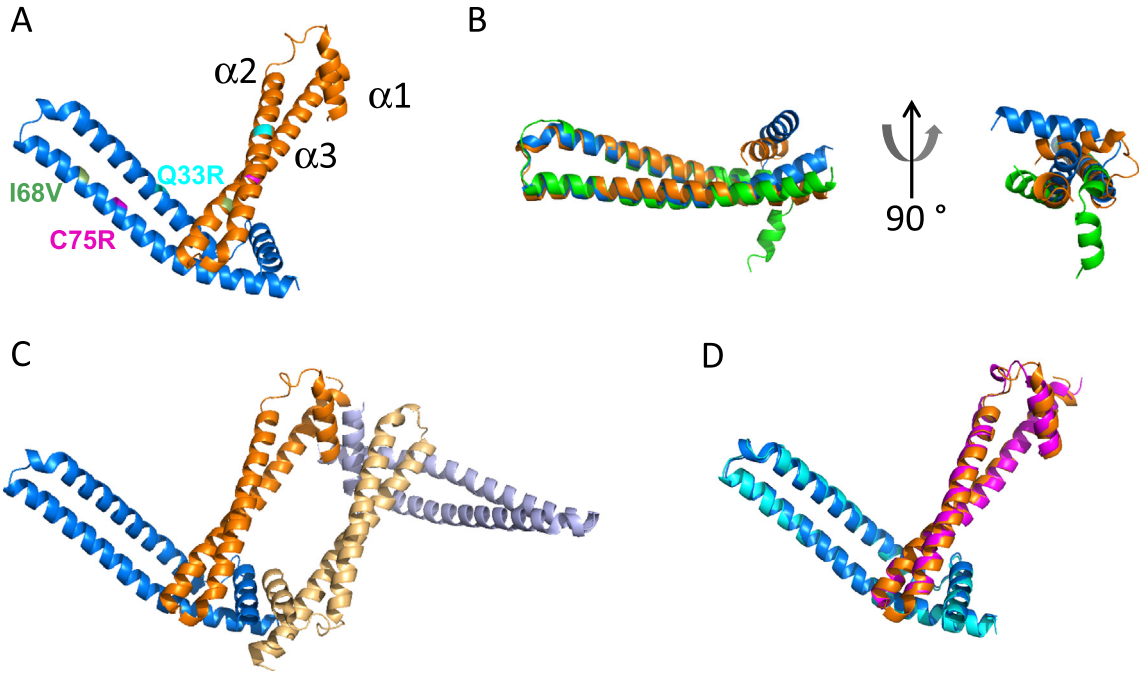

Fig. 5. Crystal structure of ING5 Nt. (A) The ING5 Nt homodimer in the asymmetric unit of the crystal. The two protomers are shown as ribbons with orange (open) and blue (closed) color. The three helices from each protomer are indicated in the open protomer, and the position of the three mutants detected in primary tumors are indicated in the closed protomer. (B) Two views of the superposition of the two protomers of ING5. The structure of the protomer of ING4 is also superposed and shown as a green ribbon by alignment of residues in helices α2 and α3. (C) Ribbon diagram of the tetramer found in the crystal by PISA analysis. The chains of the second dimer are depicted in paler colors. (D) Structure of the ING5 Nt C19S homodimer in the asymmetric unit of the crystal, with the two protomers shown as ribbons with magenta (open) and cyan (closed protomer) and superposed on the corresponding dimer of the wild type.

The asymmetric unit of the crystal contained two polypeptide chains that form a homodimer, together with several molecules coming from the buffer and cryoprotectant solution. The dimer is formed by two protomers, which correspond to chains A and B in the Protein Data Bank (PDB) file (colored orange and blue, respectively, in Fig. 5A). Each of the two chains forms a helix–loop–helix structure with two long helices (residues 19–52 and 58–104, named α2 and α3, respectively) plus a short α1 helix at the N-terminus (residues 0–11, with residue 0 being the Ala preceding M1). The distribution of the secondary structure along the sequence is shown in Fig. S4.

The two helices of each protomer form an antiparallel coiled-coil structure, and both helices contain sequence segments with the typical heptad pattern $(abcdefg)_n$, of coiled coils as analyzed with SOCKET [21]. However, helix α3 is bent, with a kink around residue Y90 in one protomer (chain B) but not in the other (chain A). The asymmetry between the protomers is clearly seen in the superposition based on helices α2 and α3 of both chains (Fig. 5B). They differ not only in the bending of helix α3 but also in the relative position of helix α1 with respect to the other two. In the dimer, the region of chain B where the short α1 is located closes around the α2–loop–α3 region of chain A (Fig. 5A). For this reason, we name the chain B the closed protomer and chain A the open protomer.

The two protomers share many intramolecular interactions, including long-range ones like the inter-helical salt bridge D32–K82 (Fig. S5A). But there are also interactions formed only in one of the protomers, some of them involving residues in the N-terminal region. For example, the salt bridge H9–D101 and hydrogen bond S13–H96, which are only formed in the closed protomer, and the salt bridge between the amine group of G-1 (preceding A0, both residues present as a result of the cloning) and D94, which is only present in the open protomer (Fig. S5A).

The crystal structure of the ING5 Nt is unexpected because of its asymmetry, which is inconsistent with the NMR observations. The global asymmetry of the structure was quantitatively evaluated [22] yielding a value of 23.21 Å (as compared with 0.06 Å for the dimer of ING4). The intermolecular packing at the homodimer interface involves the helix–loop–helix end of the open protomer and the other end of the closed protomer. This mode of packing results in two separated hydrophobic cores: the intramolecular three-helical hydrophobic core of the open protomer, and the intermolecular five-helical hydrophobic core

(Fig. 5A). These two hydrophobic cores are small for a protein of this size. In fact, the PISA analysis of the crystal suggests a tetramer as the most stable quaternary structure in solution. This putative tetramer consists of two dimers arranged so that the α1 helices of one dimer pack in an antiparallel way against the α1 helices of the other dimer, as shown in Fig. 5C. Each of the two α1–α1 interfaces is stabilized by a network of intermolecular salt bridges and hydrogen bonds. The side chain of E8 in the α1 helix of the closed protomer in one of the dimers interacts with the backbone amide of M1 and A2 in helix α1 of the open protomer in the other dimer (acting as an intermolecular N-cap residue of the second helix α1) and forms a salt bridge with the N-terminal amine of G-1 in the same helix (Fig. S5B). At the same time, the side chain of D101 of helix α3 in the open protomer acts as an intermolecular helix N-cap of the first α1 helix (in the closed protomer of the other dimer), with H-bonds to M1 and A2, and also forms a salt bridge with the amine group of G-1 (Fig. S5B). This interface is, according to PISA criteria, as significant as the interface seen in the asymmetric unit of the crystal (the five helix hydrophobic core described above), suggesting that it may also exist in solution. However, SEC-MALS experiments show that ING5 Nt forms only dimers.

One possible explanation for the inconsistency is that the presence of two extra residues at the N-terminus favors interactions that in the crystal result in the formation of a dimer of asymmetric dimers. Another possibility may be the close contact of C19 side chain of one ING5 Nt molecule and the corresponding C19 side chain of a symmetry related molecule. In fact, the refinement of the structure provides two alternative orientations (with 70%–30% occupancy) for C19, in the minor one with the geometry of an intermolecular disulfide bridge (Fig. S5C). There were no other contacts in the crystal lattice that could explain the formation of the unexpected crystal structure. To investigate the source of the inconsistency between the crystal and solution results, we examined two mutants: an N-terminal mutant that lacks the two extra residues coming from the cloning procedure ($ING5_{2-105}$, lacking also the initial methionine) and the point mutant C19S (which cannot form any disulfide bridges). The two proteins formed dimers in solution with coiled-coil structure, as seen by CD and SEC-MALS (Fig. S6). $ING5_{2-105}$ did not crystallize, but its NMR spectrum is very similar to that of ING5 Nt, with the main differences appearing at signals close to the N-terminal residues (Fig. S7). The C19S mutant formed crystals in slightly different conditions than Nt (pH 7.5 instead of 6.5), but the structure is essentially the same as the wild type: an asymmetric dimer (Fig. 5D and Fig. S5D) that could form symmetric tetramers, according to PISA. These results indicate that the cause of the ING5 Nt adopting an asymmetric dimer structure in the crystal is not the presence of a disulfide bond. In light of all the results it appears likely that the reason for the asymmetric structure is the presence of extraneous residues at the N-terminus that may favor interactions that in the crystal result in the formation of a dimer of asymmetric dimers.

The structure of ING5 Nt was examined in solution by small-angle x-ray scattering (SAXS). As the crystallography model of ING5 Nt differs in the overall shape from the model based on the crystal structure of ING4, SAXS can discriminate between these two possible dimers. The SAXS measurements show that the Nt domain has a defined structure. The Kratky plot displays a pronounced peak that indicates that it is a folded protein (Fig. S8). The distance distribution function, $p(r)$, of Nt was calculated with a maximum particle length of 89 Å and a radius of gyration of 25 Å, values similar to those measured for the ING4 Nt [15]. A low-resolution *ab initio* structural model of the ING5 Nt domain based on the SAXS data shows an elongated molecule (Fig. 6A). The fitting of the SAXS envelope (Fig. 6B) is better for the symmetric model (χ^2 = 1.8) than for the asymmetric crystal structure (χ^2 = 9.8), indicating that in solution the structure of the dimer is similar to the symmetric model. The SAXS data of the C19S yield a similar elongated volume as the wild type and fits better the symmetric than the asymmetric model (χ^2 = 2.0 and 12.0 Å, respectively; Fig. 6C and D). Together with the SEC-MALS, CD, and NMR data, we interpret these results as ING5 Nt folded as a helix–loop–helix structure that dimerizes into a symmetric four-helix coiled coil, with a flexible N-terminal tail populating a transient short helical structure.

We took advantage of the two native cysteine residues in ING5 Nt, which can be labeled with the paramagnetic tag MTSL, to further evaluate the two structural models by means of NMR paramagnetic relaxation enhancements (PREs). An initial assessment of a doubly MTSL-labeled wild type sample resulted in very poor spectra. C19 is solvent exposed in both the crystal structure (asymmetric dimer) and the model based on the ING4 Nt structure (symmetric dimer). Therefore, this is a suitable site to introduce an MTSL tag without perturbing the structure of the protein. C75, however, is partially buried or buried in the crystal structure or in the symmetric model, respectively, and the introduction of the label destabilizes the structure. Thus, we studied the C75S mutant labeled with MTSL at C19. As can be seen in Fig. 7, this protein shows a pattern of PREs that is more consistent with the symmetric dimer than with the asymmetric one.

Homo- and heteromerization of ING5 inside living cells

To confirm that ING5 forms dimers not only as a pure protein in solution but also inside the cell, we performed experiments in human embryonic kidney

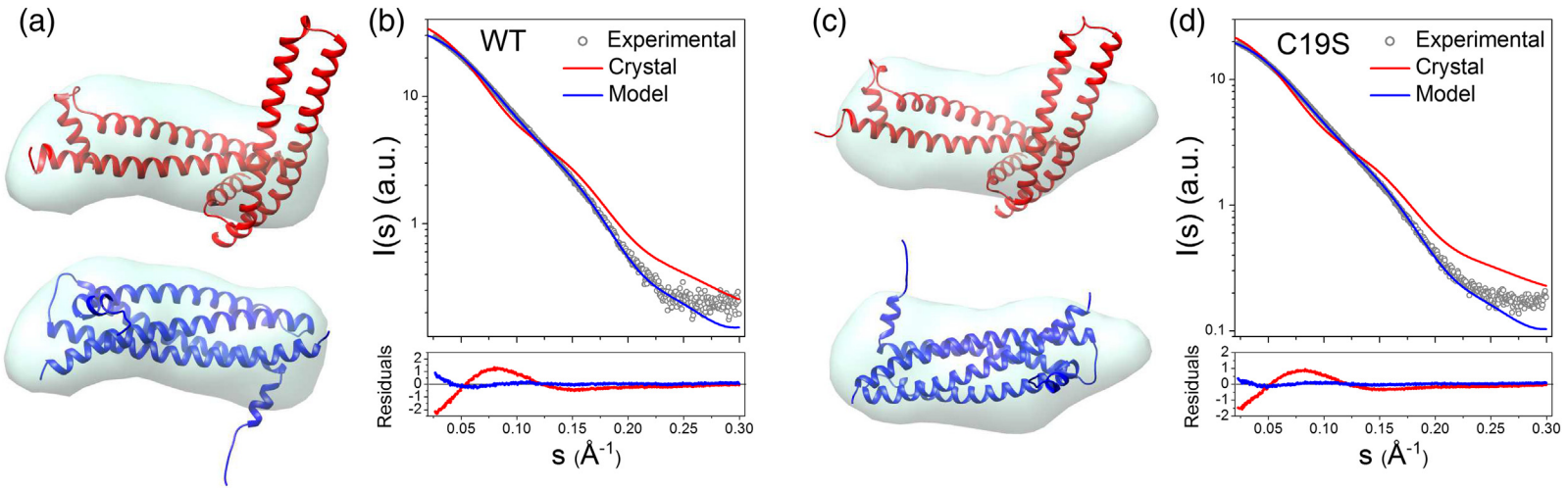

Fig. 6. Low-resolution structure of ING5 Nt dimer in solution observed by SAXS. (A) Shape reconstruction of the ING5 dimer showing the fit with the crystal structure (top panel, structure in red ribbon) or the homology-based model (bottom panel, model in blue ribbon). The radius of gyration R_g = 25 Å, and maximum particle distance is D_{max} = 89 Å. (B) Comparison of the experimental scattering (gray circles) with that calculated for the dimer in the crystal (red, χ^2 = 9.8) or the homology model dimer (blue, χ^2 = 1.8). (C) Same as in panel A for the C19S mutant (R_g = 25 Å, D_{max} = 89 Å. (D) Same as in panel C for the C19S mutant (χ^2 = 12.0 and 2.0 Å for the crystal and the model structures, respectively).

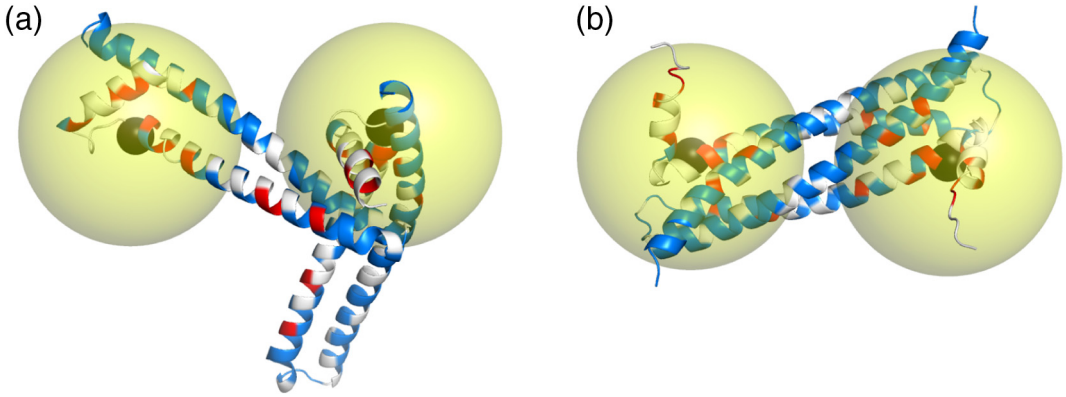

Fig. 7. PREs of the NMR signals of ING5 Nt C75S labeled with MTSL at residue C19. The ribbon of the structure modeled on the crystal structure of the WT (A) or on the crystal structure of the ING4 paralog (B) is shown in blue. The residues experiencing the largest PREs are in red, and residues for which no data are available are in gray. The location of the MTSL spin labels is indicated by black spheres in each protomer. Yellow spheres with a 10-Å radius are shown as a visual guide for the proximity to MTSL.

epithelial 293T (HEK293T) cells transiently expressing ING5 with N-terminal tags HA or AU5. We found that HA-ING5 co-precipitated with an antibody anti-AU5 tag, and that AU5-ING5 specifically co-precipitated with an antibody anti-HA tag (Fig. 8A). These results indicate that at least two ING5 molecules interact in cells.

The possibility that ING5 and ING4 could form heterodimers arises from the high-sequence identity at their Nt domains (75%) and their shared role in the HBO1 complex [10]. Since ING5 Nt is a symmetric dimer in solution, as is ING4 Nt, some inter helical interactions could be conserved in the ING5/ING4 heterodimer stabilization. An ING5/ING4 heterodimer model based on the ING4 crystal structure shows a conserved overall distribution of hydrophobic and polar residues [16], and the heptad pattern typical of coiled coils is very similar in the modeled structure of ING5 homodimer and in the crystal structure of ING4. Moreover, the intermolecular salt bridge and hydrogen bond between residues at positions D32/K39 and D94/Q69 present in the ING4 homodimer could also be established in the heterodimer [16].

The formation of heteromers inside cells was observed by co-immunoprecipitation experiments. HEK293T cells were cotransfected with vectors expressing both ING5 and ING4 but with different tags (HA or AU5), then the extracts were immunoprecipitated with the AU5 tag and blotted with the HA tag. With this strategy, co-precipitation of ING5 or ING4 will only occur if they interact. These experiments (Fig. 8B) show that ING5 and ING4 can form heteromers (most likely heterodimers), or at least that they form part of the same complex inside the cells. We tried to observe heterodimer formation with the recombinant proteins or the isolated Nt domains by sequential purification using Ni^{2+} and Strep affinity chromatography, as described [23], but we could not detect the heterodimers. These results indicate that the heterodimer is much less stable in solution than the homodimers and suggest that in cells, it may be stabilized by other proteins or by posttranslational modifications. The formation of heterodimers of the Nt domains was observed by ion mobility coupled to electrospray ionization–mass spectrometry (ESI-IM-MS) on a sample with equimolar amounts of the two Nt domains (Fig. S9 and Table S1), but with very low levels relative to the dimers or dissociated monomers and comparable to heterotrimers. Although the ionization of the protein in the gas phase may distort the behavior of the molecules, these results indicate that the isolated Nt domains can also form heterodimers.

ING5 mutants described in cancer are less stable than wild-type, inhibit cell proliferation and disrupt the cell cycle

Three tumor-specific somatic mutations in the Nt domain of ING5 have been described in oral squamous cell carcinoma [24]. These mutations are Q33R, I68V, and C75R and are located in the long helices α2 and α3. The three mutant Nt domains form dimers in solution (Fig. 1A) and adopt folded helical structures similar to that of the wild type (Fig. 2B). However, their stability, as measured by thermal denaturation, is markedly different (Fig. 2C). The Q33R mutant behaves similarly to the WT, as expected for a solvent exposed polar residue mutated into another polar residue, but both the I68V and C75R mutants involve partially buried residues and their mutation for a smaller or a larger charged residue, respectively, cause a dramatic structural destabilization. Interestingly FOLDX [25] predicts that the C75R mutation stabilizes the Nt

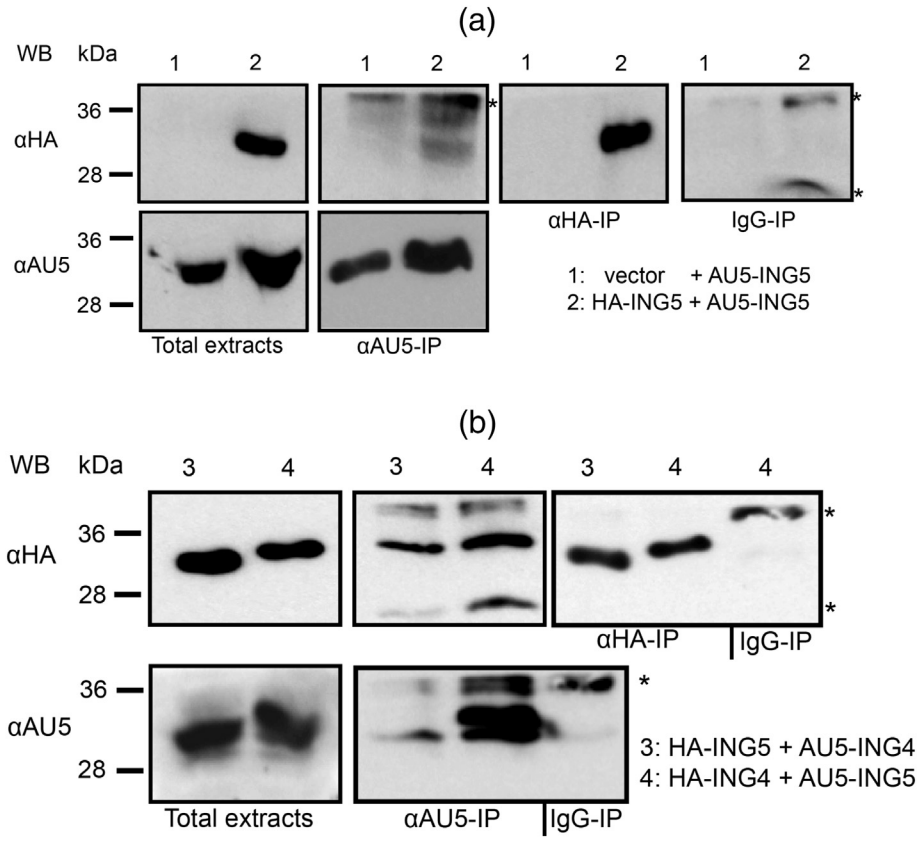

Fig. 8. (A) Analysis of ING5 association inside living cells by immunoprecipitation. Extracts from HEK293T cells transiently transfected with vectors expressing AU5-ING5 (1) or both AU5-ING5 and HA-ING5 (2) were immunoprecipitated with anti-AU5 (αAU5-IP), and the presence of the homodimer was probed with anti-HA (αHA; top middle–left panel). The immunoglobulin immunoprecipitation (IgG-IP) shows two unspecific bands (indicated with asterisks). (B). Analysis of ING5 heteromerization with ING4 in cells by co-immunoprecipitation. Extracts from HEK293T cells transiently transfected with vectors expressing HA-ING5 and AU5-ING4 (3) or HA-ING4 and AU5-ING5 (4) were immunoprecipitated with anti-AU5 (αAU5-IP) and the heterodimer visualized with anti-HA (αHA; top middle panel). Unspecific bands are indicated with asterisks.

when using the asymmetric crystal structure. However, when using the symmetric dimer model (built on the ING4 crystal structure, where C75 is buried), the prediction is that C75R strongly destabilizes the structure, as experimentally observed. For I68V (buried in the symmetric model and partially buried in the asymmetric one), a similar strong destabilization is predicted for both models.

To quantify the effect of the mutations on dimer formation, we measured the dissociation constants. Assuming a two-state transition and that dimer dissociation and protomer coiled-coil unfolding are coupled events (as indicated by the single transition observed in the melting curves) it is possible to calculate the K_d at a given temperature from the variation of the mid-point denaturation temperatures with the protein concentration [26,27]. The thermal denaturation curves are shown in Fig. S10 and the fitting of the melting temperature with the protein concentration in Fig. S11. For the WT, $K_d = 4.1 \pm 0.7$ nM, and for the Q33R mutant, $K_d = 0.4 \pm 0.3$ nM. The stabilization by introducing a polar and positively charged residue is consistent with Q33 being a solvent exposed residue close to the E36 and D37 residues, with which it can make helical stabilizing contacts ($i,i+3$ and $i,i+4$ interactions, respectively). These interactions may occur both in the symmetric and the asymmetric structural models. However, for the I68V and C75R mutants, the K_d values are almost 3 orders of magnitude larger (1400 ± 200 and 2700 ± 500 nM, respectively). The large destabilization of these mutations is consistent with both residues being completely buried in the symmetric model (while they are only partially buried in the asymmetric one).

To explore the possible functional relevance of these mutations, we measured their effects on cell proliferation. As reported for other cells [28], overexpression of ING5 had a minor effect on proliferation of NIH3T3 cells, as had the more stable Q33R mutant. However, the two destabilized mutants, I68V and C75R, showed a large inhibitory effect on cell

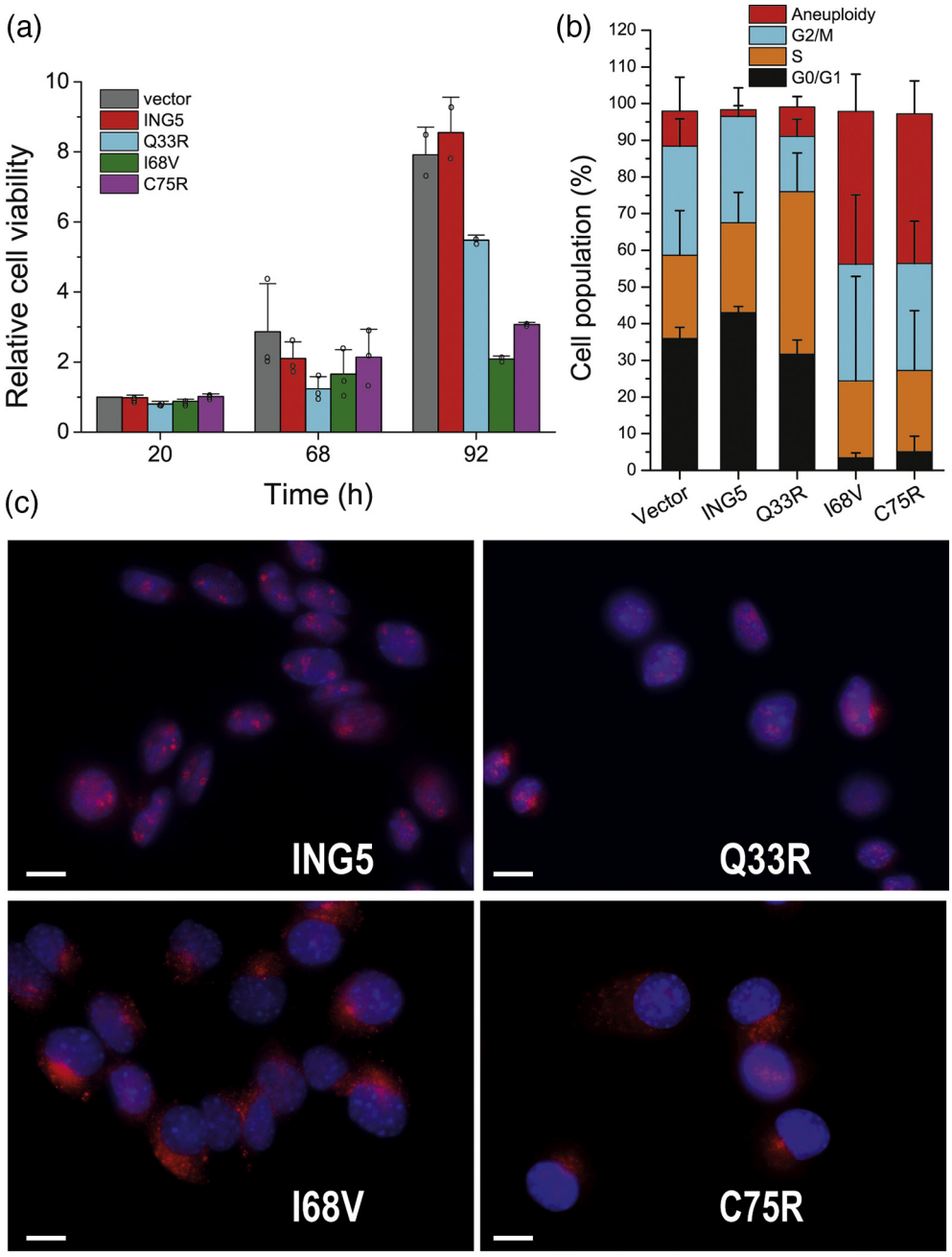

Fig. 9. (A) Proliferation difference fold of viable cells stably expressing ING5 or its mutants at different times after plating. The data are represented as bars corresponding to the mean ± S.D. of three independent experiments (n = 3, except for the 92-h experiment, where n = 2) done in quadruplicate, and the independent data are represented as scattered open circles. The reduction in cell viability is significant for the three mutants as compared with the wild type ($p < 0.05$). (B) Analysis of cell cycle distribution of cells stably expressing ING5 or its mutants. The reduction in G0/G1 cells with respect to ING5 is significant for the three mutants ($p = 0.0096$ for Q33R and $p < 0.0001$ for I68V and C75R). Aneuploidy is significantly higher in cells expressing I68V ($p = 0.025$) and C75R ($p = 0.0017$). (C) Wild-type ING5 and mutant proteins (red) detected by confocal microscopy in transfected cells; DAPI staining of nuclei is in blue. The scale bars represent a length of 10 μm.

proliferation (Fig. 9A). These results suggest that these two single point mutants act as dominant negatives, perhaps because they are not able to form a stable interaction with another ING5 molecule or interact with ING5 or one of its binding partners, resulting in inhibition of endogenous ING5 activity.

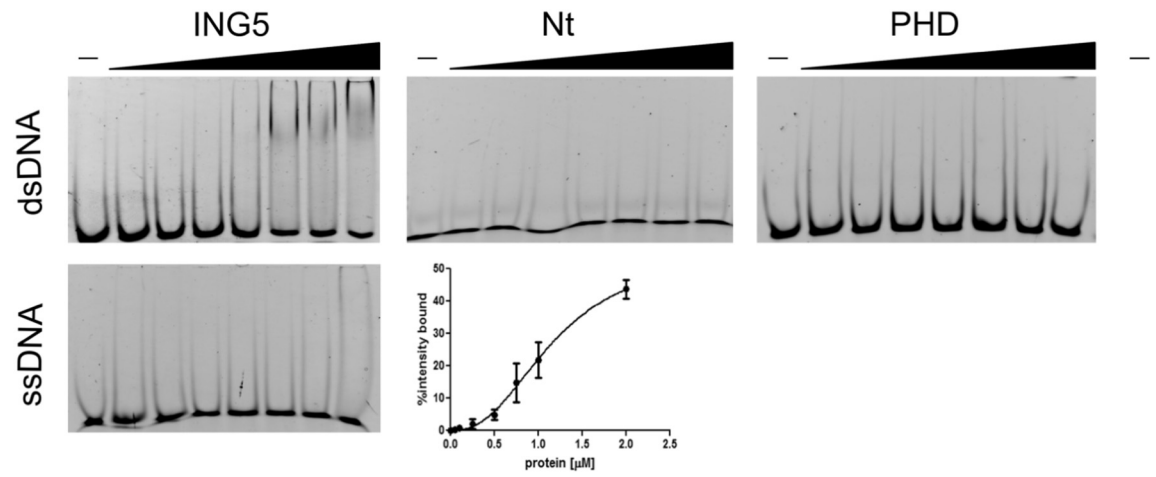

Fig. 10. (Top) Titration of dsDNA with increasing amounts of ING5 proteins and monitoring complex formation by EMSA. The concentration of DNA was 0.1 μM, and the protein concentration was (lanes from left to right) 0, 0.05, 0.1, 0.25, 0.5, 0.75, 1, and 2 μM. (Bottom) Titration of ssDNA of the same length as the dsDNA with ING5. The bottom right panel shows the quantification of dsDNA binding (closed circles) and the fitting to a Hill equation (solid line). The symbols and error bars correspond to the mean and standard deviations from three independent experiments.

This interpretation assumes that endogenous ING5 is important for proliferation in this assay, and indeed, ING5 HAT complexes have been described to be important for DNA replication [10]. Furthermore, the differential effect of the ING5 mutants could also be observed in the cell cycle distribution (Fig. 9B). Overexpression of ING5 did not alter the distribution of cells as compared with the control, and the Q33R mutant caused a small increase of cells in S phase. However, expression of the two most destabilized mutants, I68V and C75R, led to a strong reduction of cells in G0/G1 phase, accompanied by an increase in aneuploidy, above that already found in NIH3T3 cells [29]. These data suggest that ING5 function is not largely affected by the Q33R mutation, while the mutants C75R and I68V disrupt the cell cycle. Moreover, we noted that the subcellular localization of the I68V and C75R mutants was predominantly cytoplasmic, in contrast to wild-type ING5, which showed a punctate nuclear staining pattern (Fig. 9C). Thus, the ING5 dimer destabilizing mutations affect ING5 localization and activity.

The central NLS region of ING5 binds dsDNA

We have recently shown that the central NLS region of ING4 binds double-stranded DNA with micromolar affinity [30]. Because the central region of ING5 contains a similar number and distribution of positively charged residues as ING4, we hypothesized that ING5 will also bind DNA through its NLS region. The results of electrophoretic mobility shift assay (EMSA) show that the full-length protein binds dsDNA weakly, while the Nt domain and the PHD finger do not bind (Fig. 10).

The dimeric nature of ING5 makes it possible that the dsDNA binds more than one ING5 dimer. The weak binding and the multiple possible modalities of binding make it difficult to quantify and interpret the affinity of the interaction. An attempt to do so using a Hill equation [31] yields an apparent dissociation constant of 1.2 ± 0.4 μM (Fig. 10). ING5 does not appreciably bind single stranded DNA.

Discussion

Sequence analysis indicates that the ING5 conserved domains (Nt and PHD) are folded, while the non-conserved central NLS region is not [5]. Our results show that the Nt domain is folded and dimeric and indicate that the NLS region is disordered. This region tethers the PHD to the Nt domain, but its length and flexibility confer a high degree of mobility to the PHD finger with respect to the Nt. In consequence, the assignment of many of the backbone NMR signals of the PHD could be transferred to the well resolved regions of the ING5 spectrum by matching the chemical shifts of the corresponding signals. The presence of a single set of signals for all the identified amino acids indicates that the two PHD fingers of the dimer are chemically equivalent. Therefore, the ING5 dimer has two identical and independent binding sites for H3K4me3 tails which, in the context of the chromatin, could belong to the same or to different nucleosomes. The assignment allows for the detailed NMR analysis of the binding of the full-length dimeric protein to H3K4me3. The chemical shift perturbations of ING5 signals upon the addition of the 15-residue long H3K4me3 peptide shows a

slightly higher affinity (K_d = 7.0 ± 2.7 μM) than the isolated PHD finger (18.4 ± 2.8 μM). This could be due to the local increased concentration of peptide in the vicinity of one PHD finger due to the presence of the other PHD in the ING5 dimer.

The bivalency of ING5 would enhance the targeting of the HAT complexes HBO1 and MOZ/MORF to chromatin sites enriched in H3K4me3 marks. The reason for this hypothesis is that two such modifications would be within the reach of the complexes, and binding to the first site will reduce the entropic cost of the second site binding, thus increasing the overall affinity [32,33]. For the same reason, two nearby H3K4me3 chromatin sites would compete favorably for HBO1 binding over distant ones.

It is not known whether all ING proteins contribute to nucleosome binding through direct protein binding to DNA, but our results indicate that this is the case for ING5, as the central disordered NLS region of ING5 directly binds DNA with a preference for double stranded DNA and an affinity in the low micromolar range.

The crystal structure of the ING5 Nt domain shows that it forms an asymmetric homodimer with each protomer folded into a coiled coil. The secondary structure is similar to ING4 Nt, but with the α1 helix, elongated by one turn. In ING4 the residues of this short helix interact with residues on other homodimers in the same or adjacent asymmetric unit, suggesting that it does not form an integral part of the dimeric coiled-coil structure, and might be a dynamic local structure stabilized in the crystal lattice. In the crystal structure of ING5, the α1 helix of the open protomer packs in an antiparallel way with the α1 helix of a closed protomer belonging to the adjacent asymmetric unit, and *vice versa*. However, this tetrameric arrangement observed in the crystal lattice is inconsistent with the structure of ING5 Nt in solution, which forms dimers. In solution, as shown by NMR, the Nt domain of ING5 forms a symmetric homodimer, and the SAXS data indicate that it forms a structure similar to the symmetric antiparallel ING4 homodimer. Therefore, we conclude that in solution, the ING5 Nt dimer is a symmetric one, similar to that of its paralog ING4 Nt. The reason for the formation of an asymmetric crystal structure may be the non-native interactions established in the crystal by the extraneous residues at the N-terminus.

Structural models of the other ING proteins suggest that they may also form homodimers, albeit with different stabilities [16]. Furthermore, the 75% sequence identity between ING4 and ING5 Nt domains (78% taking into account only the residues at the homodimer interface of ING4) and the examination of the corresponding model structure suggest that they could form stable heterodimers [16]. Interestingly, in HeLa cells both proteins form part of the HBO1 complex and are required for chromatin modification, although they play different roles in DNA replication [10]. Heterodimerization could have a regulatory role, analogous to what has been observed in transcription factors [34]. The ING5 homodimer does form inside cells and the heterodimer may form as well, as seen by coimmunoprecipitation in HEK293T cells. We have not been able, however, to confirm the stable formation of heterodimers using the purified proteins, although mass spectrometry indicates that they form transiently. These results suggest that ING4 and ING5 could form heterodimers in cells through interaction with other proteins. Alternatively, they may be part of the HBO1 complex simultaneously, as homodimers. It has been shown that domain IIb of JADE1 (one of the components of the HBO1 complex) interacts with ING4 independently of the ING4 PHD finger [78], and a similar interaction could occur with ING5.

It has been described that ING5 HAT complexes are important for DNA replication [10], and a role in self-renewal of glioblastoma stem cells has been recently described [35]. Two of the three mutations detected in primary tumors of oral squamous cell carcinoma [24] strongly destabilized the ING5 Nt structure, while the third stabilized the structure and had little effect on cell proliferation. Therefore, the two deleterious mutations might be driver cancer mutations, while the other could be a passenger mutation. Moreover, the two deleterious mutants were predominantly localized to the cytoplasm, consistent with studies showing increased cytoplasmic ING5 in colorectal cancer [36]. One possibility is that the two deleterious mutations confer dominant-negative activity, whereby the mutant proteins bind endogenous ING5 or its partners to form inactive complexes, for example, by altering subcellular localization. Decreased nuclear ING5 has been linked to tumorigenesis in head and neck squamous cell carcinoma [37], gastric cancer [38], colorectal cancer [36], and breast cancer [39]. Thus, for example, in breast cancer, cytoplasmic ING5 expression has been linked to poor prognosis [39]. In this context, it is interesting to note that miR-24, an oncomiR shown to be a direct upstream regulator of ING5, is increased in breast cancer stem cells and induces chemotherapy resistance [40], in agreement with the role of ING5 in inhibiting epithelial–mesenchymal transition in breast cancer [41].

Conclusions

ING5 is a dimeric protein that contains two identical PHD fingers that recognize histone H3K4me3 with a K_d in the micromolar range. The dimerization site is at the Nt domain, with a symmetric coiled-coil structure similar to that of its paralog ING4, while the central region is flexible and binds dsDNA. ING5 is a bivalent reader of H3K4me3, and heterodimer formation with ING4

could increase its functional diversity. Mutations C75R and I68V detected in primary tumors disrupt the cell cycle, probably due to the strong destabilization of the Nt domain structure.

Materials and Methods

Cloning and mutagenesis

The full-length human ING5 (1-240) construct (Uniprot entry Q8WYH8, isoform 1) was designed with a His_6-tag in the N-terminus for purification by affinity chromatography, followed by a TEV protease-specific sequence (ENLYFQG, which TEV cleaves after the Q residue) in order to remove the tag after purification. Between the TEV site and the initial methionine of ING5 an alanine was inserted to facilitate TEV cleavage. A synthetic gene of the full-length ING5 with codons optimized for expression in *Escherichia coli* (Entelechon GmbH) was cloned into the expression vector pET11d. The construct for the Nt of ING5 (residues 1–105, ING5 Nt) was obtained by inserting a stop codon at the site corresponding to R106 by means of mutagenic PCR. This clone was used as a template for the production of different ING5 Nt mutants: C19S, Q33R, I68V, C75R, and C75S. Mutagenesis was performed using the Quick Change kit (Agilent Technologies) with primers from Thermo Scientific. A clone of ING5 Nt without any affinity tag (producing the protein $ING5_{2\text{-}105}$ without the initial methionine) was also produced by PCR amplification.

The DNA of the C-terminal PHD of ING5 (residues 178–240) was amplified by PCR introducing NcoI and BamHI restriction sites at the 5′ and 3′ ends and cloned into a modified pET29a expression vector as follows. A synthetic gene (GenScript, USA) coding for ubiquitin with a His_{10}-tag inserted in the loop between the first β-hairpin and the helix [42] was modified to include the Strep-tag sequence and the TEV protease cleavage site at the C-terminal end of ubiquitin. This construct was cloned in pET29a, and the PHD of ING5 was then cloned after the TEV protease site. The expressed and cleaved protein contains the sequence GAM before the PHD residue D178.

For overexpression of ING5 in mammalian cells, the cDNA of ING5 was obtained from AddGene. The gene was amplified by PCR with N-terminal AU5 or HA immunotags and cloned into the pLPC retroviral vector.

The synthetic gene of the full-length ING4 (residues 1–249, Uniprot Q9UNL4, isoform 1), with codons optimized for expression in *E. coli* was previously described [15]. This construct was modified with a Strep-tag sequence at its N-terminus with two aims: simplify its purification and introduce an affinity tag orthogonal to the His-tag of ING5 Nt for the heterodimerization assays by copurification. The analogous Strep-tag construct for the Nt of ING4 (ING4 Nt, residues 2–108) was obtained by inserting a stop codon at the site corresponding to A109.

All sequences and mutations were confirmed by DNA sequencing (Stabvida, Portugal).

Protein expression and purification

All the proteins were over-expressed in *E. coli* BL21(DE3) and cells grown in LB or auto-induction rich normal medium [43]. [U-^{15}N]-labeled proteins were produced in a modified auto-induction media [44] or in minimal media as described [45]. For the production of U-^{15}N-labeled or [U-^{13}C, U-^{15}N]-labeled proteins, minimal media was used as previously described [45,46]. Cells in LB were grown at 37 °C until OD_{600} = 0.8, when expression was induced with 0.5 mM IPTG for 3 h at 37 °C. Cells in auto-induction medium were grown for 2 h at 37 °C before lowering the temperature to 20 °C for expression for 16–23 h. The cells were harvested by centrifugation and resuspended in lysis buffer [20 mM Tris (pH 8.0), 300 mM NaCl, 1 mM DTT with *Complete EDTA-free* protease inhibitors]. After sonication and ultracentrifugation, proteins were found predominantly in the insoluble (ING4, ING4 Nt, ING5, ING5 Nt, ING5 PHD, and the ING5 Nt mutants C19S, Q33R, I68V, C75R, and C75S) or in the soluble fraction (tagless ING5 Nt). Insoluble proteins were recovered from the pellets by solubilization in 8 M urea and ultracentrifugation for 3 h. Supernatant was refolded by a 50- to 100-fold dilution into cold 20 mM, Tris (pH 8.0), 300 mM NaCl, and 1 mM DTT (plus 50 μM $ZnCl_2$ in the case of the PHD or the full-length proteins for proper folding of the PHD).

Full-length ING5 was purified by immobilized metal affinity chromatography (IMAC) with a 5 mL His-Trap column (GE Healthcare) and eluted with a linear imidazol gradient (0–0.5 M) in 15 column volumes (CV). Selected fractions were loaded in a Superdex 200 26/60 in 20 mM Tris (pH 8.0), 300 mM NaCl, and 1 mM DTT. After one or more runs, the protein was judged to be pure and concentrated at about 0.7 g/L (precipitation occurred at higher concentrations). No cleavage of the His-tag was done, and the yield was 0.7 mg/L. The Nt of ING5 and all its mutants were purified by IMAC with a His-Trap column (GE Healthcare) and eluted with an imidazol linear gradient (0–0.5 M) in 5 CV. Selected protein containing fractions were incubated with in-house produced His_6-TEV protease (1 mg of protease per 30 mg of protein) and dialyzed against 20 mM, Tris (pH 8.0), 40 mM NaCl, and 1 mM DTT at 4 °C for 16 h. The sample was loaded on a His-Trap column, and the flow through was then loaded on a 5 mL Hi-Trap Q HP column (GE Healthcare). The

protein was eluted with a linear gradient of NaCl (0.04–1 M) in 5 CV. Selected fractions were concentrated and polished by gel filtration on a Superdex 75 16/60 column (GE Healthcare) in 20 mM Tris (pH 8.0), 300 mM NaCl, and 1 mM DTT. Typical yields were of 6–12 mg/L. The cells producing the soluble tagless $ING5_{2-105}$ were lyzed using a lysis buffer without NaCl, and the protein was purified by anion-exchange chromatography on a Q-Sepharose 26/10 column (GE Healthcare). The protein was eluted with a gradient from 0 to 1 M NaCl in 10 CV, and selected fractions were polished by gel filtration separation on Superdex 75 26/60 in 20 mM Tris (pH 8.0), 300 mM NaCl, and 1 mM DTT. The yield was about 30 mg/L.

ING4 and ING4 Nt were purified on a Strep-tactin 5 mL column (IBA-lifesciences) equilibrated in 100 mM Tris–HCl (pH 8.0) and 150 mM NaCl. The proteins were eluted with 2.5 mM desthiobiotin. Selected fractions were concentrated and loaded onto Superdex 200 16/60 (ING4) and Superdex 75 16/60 (ING4 Nt) equilibrated in 20 mM Tris–HCl (pH 8.0), 300 mM NaCl, and 1 mM DTT. Typical yields were 0.6 and 7 mg/L (for ING4 and ING4 Nt, respectively).

The soluble PHD finger of ING5 was purified form the soluble fraction by sequential IMAC, Strep-affinity, TEV cleavage, and gel filtration chromatography using protocols as detailed for the other constructs.

For each purified protein, the molecular weight was confirmed by MALDI-TOF and its concentration was measured by UV absorbance (with the extinction coefficient at 280 nm calculated from the amino acid sequence using the Expasy Protparam server [47]). All the proteins purified after cleavage of the affinity tags have the two extra N-terminal residues (GA), with the exception of the ING5 PHD finger, which has three residues (GAM). The tagless ING5 Nt lacks the initial methionine.

CD

These measurements were performed on a Jasco J-815 spectropolarimeter at 25 °C. The spectra were the average of five scans, recorded using a 0.1-mm path length quartz cuvette on 12 μM (ING5) or 40 μM (Nt and its mutants) protein samples in 20 mM Tris (pH 8.0), 300 mM NaCl, and 1 mM DTT. Thermal denaturation curves were measured in 2-mm path length cuvettes closed with a teflon cap on solutions with different protein concentrations (in the range of 1–40 μM). Denaturation was induced by increasing temperature at a rate of 1 °C/min from 5 °C to 95 °C, and the ellipticity at 222 nm was recorded at intervals of 0.2 °C using a 2-nm bandwidth and a response of 16 s). The midpoints of the thermal-denaturation curves (T_m) were determined from the first derivative, the second derivative, or by fitting the data to a sigmoidal transition curve. The dimer dissociation constants are reported as the average derived from the three methods with the standard deviation as an estimation of the uncertainty.

SAXS

SAXS data were collected at 20 °C on the BM29 beamline at The European Synchrotron Radiation Facility, in Grenoble, France, with a 2D detector (Pilatus 1M) over an angular range qmin = 0.01 $Å^{-1}$ to qmax = 0.5 $Å^{-1}$ [48]. Prior to measurements, the samples were loaded onto a PD10 column equilibrated in 20 mM Tris (pH 8.0), 300 mM NaCl, and 1 mM TCEP and concentrated by ultrafiltration. Aliquots of the samples were prepared by dilution at different concentrations, and the buffer was used as a blank for the SAXS experiments. The protein concentrations used were 4 and 7 g/L for ING5 Nt and 5 and 12 g/L for the C19S mutant. The analysis of the data sets at different concentrations gave similar results. Data collection, processing, and initial analysis were performed using the beamline software BsxCUBE. Further analysis was performed with ATSAS [49]. The Guinier approximation was used to calculate the radius of gyration using the PRIMUS software [50]. The distance distribution function, $p(r)$, was computed with the program GNOM [51] by optimizing the maximum particle size, D_{max}. Low-resolution *ab initio* reconstructions of the Nt domain were built from the scattering data using GASBOR [52]. Ten independent GASBOR reconstructions were performed, and the most representative model was filtered with DAMSEL [53]. The low-resolution shape of the Nt is represented as an assembly of 230 dummy residues with a maximum distance of 89 Å. The crystal structure of ING5 Nt or the homology model based on the crystal structure of ING4 Nt (PDB 4AFL) was fitted to the SAXS data with CRYSOL [54]. The goodness of the fitting is characterized by the discrepancy value χ^2. Superposition of the bead model on the structures was carried out with SUBCOMB [55] and visualized with Chimera [56]. The model of ING5 Nt on the crystal structure of ING4 Nt was built with FOLDX [25] and the three or four missing residues at the N-termini of the two protomers (absent in the crystal structure of ING4) were modeled in a non-regular conformation.

Size exclusion chromatography-multi angle light scattering (SEC-MALS)

These experiments were performed at 25 °C using a Superdex 200 10/300 GL column (GE HealthCare) connected to a DAWN-HELEOS light scattering detector and an Optilab rEX differential refractive index detector (Wyatt Technology). The column was equilibrated with running buffer [20 mM Tris (pH 8.0), 300 mM NaCl, 0.5 mM TCEP, 0.03% NaN3, 0.1 μm filtered], and the SEC-MALS system was calibrated

with a sample of Bovine Serum Albumin (BSA) at 1 g/L in the same buffer. Samples of 100 µL protein at 0.5–1.5 g/L were injected at 0.5 mL/min. We employed ASTRA software (Wyatt) for data acquisition and analysis. Based on numerous measurements on BSA samples at 1 g/L under the same or similar conditions, we estimate that the experimental error in molar mass is around 5%.

NMR spectroscopy

Spectra were recorded at 25 °C on a Bruker Avance III 800 spectrometer using a triple resonance cryo-probe equipped with z gradient coil. The ING5 Nt protein sample was prepared at 270 µM in 50 mM Mops (pH 7.3), 1 mM DTT, 10% $^{2}H_2O$, 3 µM DSS (2,2-dimethyl-2-silapentane-5-sulfonate sodium salt), and protease inhibitors. H^N, Hα, N, CO, Cα, and Cβ assignments of ING5 Nt were obtained from 2D ^{15}N-TROSY, ^{13}C-HSQC spectra and from TROSY-based 3D HNCO, HN(CA)CO, HNCA, HN(CO)CA, HNCACB, HN(CO)CACB, HN(COCA)HA, and HN(CA)HA. NMR spectra of the PHD finger were recorded on a sample with a protein concentration of 215 µM in 20 mM Tris (pH 8.0), 300 mM NaCl, 1 mM DTT, 5% $^{2}H_2O$, and 3 µM DSS. The assignment of the PHD finger of ING5 was obtained from 2D ^{15}N-TROSY, ^{13}C-HSQC spectra and from TROSY-based 3D HNCO, HN(CA)CO, HNCA, HN(CO)CA, HN(CA)HA, HN(COCA)HA HNCB, and HNCACB, experiments acquired with non-uniform sampling [57].

Chemical shifts were measured relative to internal DSS for ^{1}H and calculated for ^{15}N and ^{13}C [58]. NMR data were processed with TOPSpin (Bruker), except those acquired with non-uniform sampling, which were processed with MddNMR [57]. NMR spectra were analyzed using Sparky (Goddard and DG Kneller, University of California, San Francisco). Spectral assignment was initially done automatically using MARS [59] and manually completed. The NMR assignments have been deposited in the BioMagResBank under accession codes of 27653 for $ING5_{1–105}$ and 27654 for the PHD finger.

The synthetic peptide H3K4me3 corresponds to residues 1–15 of histone H3 plus an extra tyrosine residue at the C-terminus (ARTKQTARKSTGGKAY) to measure peptide concentration by ultraviolet (UV) absorbance. This peptide has free N- and C-termini and was purchased from PolyPeptide. The titration of ING5 and the PHD with the peptide and the NMR binding analysis was performed as previously described for ING4 [60] on 10 µM samples in 20 mM Tris (pH 8.0), 300 mM NaCl, 1 mM DTT, 5% $^{2}H_2O$, and 3 µM DSS. Perturbed residues were considered when the combined ^{1}H and ^{15}N chemical shift perturbation (calculated as $CSP = ((\Delta\delta_H)^2 + 0.2(\Delta\delta_N)^2)^{1/2}$, where Δδ stands for the shift caused by the presence of the peptide) was larger than the average plus one standard deviation. The individual dissociation residue constants, derived from the fitting of the data to a single set of binding sites, yield constants that are reported as the average over the perturbed residues with the standard deviation as an estimation of the uncertainty.

For NMR PRE measurements on ING5 Nt labeled at C19 (using the C75S mutant), the buffer was exchanged to 50 mM Mops (pH 7.0) with a desalting PD10 column to remove the DTT. The protein was concentrated by ultrafiltration to 200 µM and divided in two halves. One half was supplemented with 1 mM DTT and was used as the reference sample (diamagnetic, absence of spin label). The other half of the sample was labeled using a 6-fold molar excess of MTSL ((*S*-(1-oxyl-2,2,5,5-tetramethyl-2,5-dihydro-1*H*-pyrrol-3-yl)methyl methanesulfonothioate)) at 25 °C for 2 h in the absence of light [61]. The homogeneity of the protein and the presence of the covalently bound MTSL moiety were confirmed by MALDI-TOF mass spectrometry. Prior to NMR experiments, 5% $^{2}H_2O$ and 3 µM DSS were added to the samples. The overall PRE effect was measured in ^{1}H–^{15}N TROSY spectra acquired and processed under identical conditions. The intensity ratio of the cross-peaks in the presence and absence of the cysteine-attached spin label were measured, and those experiencing a large intensity reduction in the MTSL labeled protein (up to the 40th percentile) were selected as the most perturbed residues.

Crystallization, data collection, and structure solution

Initial crystallization plates were performed in sitting drops at 21 °C with a Mosquito robot (TTP, Labtech) in 96-well MRC plates (Molecular Dimensions) using the vapor diffusion technique. A total of 1800 different crystallization conditions from commercial sources (Molecular Dimensions, Hampton Research, and Qiagen) were tested. Drops consisted of 0.1–0.3 µL protein solution at 20 g/L [in 20 mM Tris (pH 8.0), 300 mM NaCl, 1 mM DTT] plus 0.1–0.3 µL reservoir solution and a reservoir volume of 60 µL. Crystallization conditions were manually optimized with drops made of 1 µL protein and 1 µL reservoir solution. Best crystals for ING5 Nt were obtained in 0.1 M Mes (pH 6.5), 22% (v/v) MPD, and 5% PEG3350. Crystals were cryoprotected with 20% ethylenglicol and diffraction data were collected at 3.2-Å resolution at the XALOC beamline at the ALBA synchrotron (Table 1).

Crystals of the ING5 Nt C19S mutant obtained in conditions very similar to the wild type were very fragile and did not diffract. New crystals were obtained in 0.1 M sodium Mops/Hepes (pH 7.5), 37.5% MPD_PEG1K_PEG3350, 0.03 M $NaNO_3$, 0.03 M Na_2HPO_4, and 0.03 M $(NH_4)_2SO_4$). The reservoir solution was a good cryoprotectant

condition. Diffraction data were collected at PROXIMA1 beamline in SOLEIL synchrotron in a DECTRIS PILATUS3 6M detector, at 3.1 Å (Table 1). Crystals of ING5 $Nt_{2\text{-}105}$ were obtained in several conditions, all containing jeffamine M-600, but did not diffract.

The ING5 Nt diffraction data set was indexed, integrated, and scaled using HKL2000 [62]. PHASER [63] was used to determine the structure of ING5 Nt by molecular replacement using ING4 Nt (PDB 4AFL) as a search model. All side chains of the ING4 Nt structure (A–F) were processed in CHAINSAW [64] to obtain a model that preserved side-chain atoms shared by both ING5 Nt and ING4 Nt sequences. The most flexible regions of the structure of ING4 Nt were eliminated in COOT [65], leaving only regions corresponding to residues 14–51 and 62–105 from chains A–F. The superposition of these chains was used as the final model in PHASER from CCP4 [66] for the molecular replacement in $P6_122$ and $P6_522$. The final ING5 Nt model was obtained from the PHASER model in the latter space group after some cycles of manual construction with COOT and the Autobuild routine in BUCCANEER [67], followed by refinement cycles in autoBUSTER [68]. Diffraction data from the C19S mutant were processed with MOSFLM [69] and scaled with SCALA [70]. The crystal structure of the wild type was used for molecular replacement with MOLREP [71]. The final model was reconstructed with COOT [65] and refined with REFMAC [72].

The final structural models were validated for geometry and stereochemistry restrictions [73] with MOLPROBITY [74], and were analyzed with PISA [75] and Socket [21]. Figures were produced with PYMOL [76]. The coordinates and structure factors have been deposited at the PDB with the entry codes 5ME8 (ING5 Nt wild type) and 5MTO (C19S mutant).

ESI-IM-MS

Samples of Strep-ING4 Nt and ING5 Nt proteins were buffer exchanged into 100 mM ammonium acetate (pH 6.9) using a PD-10 column and concentrated by ultrafiltration. Three samples (the two individual proteins and the equimolar mixture of both) were incubated at 85 μM (total protomer concentration) in a volume of 200 μL overnight at 37 °C. Before injection, the samples were further desalted on a Micro Bio-Spin 6 column (Biorad) using ammonium acetate 100 mM as the exchanging buffer. ESI-IM-MS experiments were conducted on a Synapt HDMS (Waters) quadrupole-traveling wave IMS-oaTOF mass spectrometer equipped with an Advion TriVersa NanoMate (Advion Biosciences). Mass spectra were recorded under non-denaturing instrumental conditions in the positive ion mode. The Advion source was working in direct infusion mode allowing automated chip-based nanoelectrospray. Spray voltage was 1.75 kV, and delivery pressure was 0.5 psi. Backing pressure, sampling cone voltage, trap collision energy, transfer collision energy, and source temperature were set to 5.83 mbar, 40 V, 6 V, 4 V, and 20 °C, respectively. The IM gas flow was kept at 23 mL/min, gas pressure in ion mobility cell at 4.49×10^{-1} mbar, and gas flow rate in the trap cell at 5 mL/min. Wave height and wave velocity in the ion mobility cell were set to 9 V and 350 m s^{-1}, respectively. External mass calibration was achieved using a cesium iodide solution in m/z range of 500 to 8000. Data were acquired and processed with MassLynx software v 4.1 (SCN 704). MS spectra were deconvoluted to the average masses with integrated algorithms in MassLynx, and IM-MS data were processed with Driftscope software version 2.4.

Cell cultures, plasmids, and transfection

Human cell line HEK-293T (embryonic kidney epitelium) and immortalized mouse fibroblasts NIH3T3 were cultured in DMEM (Gibco) or in RPMI medium (Gibco), all suplemented with 10% FCS and penicillin/streptomycin at 37 °C and 5% CO_2. Cells were passaged when they reached 70%–80% confluence at 1:5–6 with 0.05% trypsin. Transfection of HEK-293T and NIH3T3 cells was performed using a standard calcium phosphate method after seeding 3×10^6 cells on 10-cm plates. Selection of stably transfected NIH3T3 cells was performed at 2 μg/mL puromycin during 2 to 3 weeks after transfection, and the antibiotic was mantained in the medium at a low dose (0.5 μg/mL).

Cell proliferation and flow cytometry analysis

To evaluate and compare the effect in cell proliferation in stably transfected NIH3T3 expressing ING5 or its mutants, 2000 cells per well were seeded in 96-well plates and allowed to grow for different times. Then, cells were rinsed with phosphate-buffered saline (PBS) and stained using crystal violet. The stain was solubilized in 10% acetic acid after air drying and diluted in water for absorbance measurement at 595 nm. Three independent experiments were done in quadruplicate. The significance of the results was evaluated by the Student's *t*-test.

To analyze the cell cycle phase distribution, NIH3T3 cells stably expressing ING5 and its mutants were harvested prior to confluence from a 6-well plate, fixed with 70% (vol/vol) ethanol, and stored at −20 °C for overnight. After ethanol was removed by centrifugation, pellets were resuspended in PBS containing 40 μg/mL propidium iodide and 100 μg/mL RNase A, and incubated for 30 min at room temperature. The DNA content was measured as the propidum iodide signal to determine cell cycle profiles using FACSCanto (BD Biosciences) and

then analyzed by FACS Diva software. At least 20,000 cells were analyzed from each sample. NIH3T3 cells already show aneuploidy [29]; however, the level of aneuploidy in our stock of NIH3T3 cells and vector control cells was much lower than that in cells expressing the ING5 mutants. The significance of the results was based on the Student's *t*-test.

Immunoprecipitation and Western Blot analyisis

Whole-cell extracts were prepared from transfected HEK-293T cells grown on a 10-cm plate. Cells were lysed in 1 mL of ice-cold radio-immunoprecipitation assay buffer (Millipore) supplemented with 0.1% SDS and Complete (Roche) protease and phosphatase inhibitor mixture tablets as previously described [77]. For immunoprecipitation, mouse monoclonal anti-HA (12CA5 clone; Roche) and mouse monoclonal anti-AU5 (Abcam) primary antibodies were used. One microgram of the antibody was incubated with ~1 mg of the lysate for 16 h at 4 °C. Next, 20 µL of BSA blocked agarose-conjugated protein A/G beads (Santa Cruz) were incubated with extracts for 1 h at 4 °C, and after washing three times with radio-immunoprecipitation assay buffer, samples were probed by Western blotting. Samples were resolved by 10% SDS-polyacrylamide gel electrophoresis and transferred onto Protran® (Whatman) nitrocellulose membranes with 0.45-µm pore size. Nonspecific binding was blocked by 1-h incubation with blocking buffer before membranes were incubated overnight at 4 °C with primary antibodies diluted in blocking buffer (5% milk in Tris-buffered saline without Tween-20). After extensive washing with TBS plus 0.1% Tween-20, specific bands were detected on Hyperfilm™ (GE Healthcare) using horseradish peroxidase-conjugated goat anti-mouse Fcγ fragment-specific secondary antibody (1:10,000; Jackson Immunoresearch) and the ECL detection system (Biorad).

Immunofluorescence staining

NIH3T3 cells stably expressing ING5 and its mutants were plated in coverslips in 24-well plates at a density of 40,000 cells per well. Cells were fixed with 4% paraformaldehyde in PBS for 20 min at RT, then treated with 0.1% Triton X-100 in PBS for 10 min at RT, for membrane permeabilization and incubated for 1 h in blocking solution (2% BSA in PBS, 0.01% NaN3, glycine 50 mM). ING5 and mutants were detected with anti-HA (12CA5 clone; Roche). Primary antibody was diluted 1:200 in blocking solution. The secondary antibody used was Alexa Fluor 594 antimouse (Invitrogen A11005, dilution 1:5000). Washing between the different steps was carried out with PBS. Cells were finally mounted on to microscope slides using Vectashield containing DAPI (Vector). Slides were examined using a Zeiss Axiimager D1 fluorescence microscope.

Fluorescence EMSA

Oligonucleotides were designed to generate single-strand (ss) and double-strand (ds) DNA ligands (32 nt or 32 bp long) labeled with 6-carboxyfluorescein (6-FAM) at the 5′ end. To avoid any quenching effect, the dsDNA has two extra bases at the 5′ end. The sequences correspond to oligonucleotides A3 and B2 previously used for the same EMSA experiments with ING4 [30]. Oligonucleotides were chemically synthesized and HPLC-purified by Thermo Scientific or Sigma-Aldrich, and were solubilized in Tris–EDTA buffer [10 mM Tris–HCl (pH 8.0), 1 mM EDTA] to a concentration of 100 µM. For the preparation of the different dsDNA ligands, labeled:unlabeled oligonucleotides (in a 1:1.2 molar ratio) were mixed and diluted in annealing buffer [50 mM potassium acetate, 20 mM Tris-acetate, 10 mM magnesium acetate, 1 mM DTT (pH 7.9)] to the desired final concentration. Annealing was performed by incubation in boiling water for 5 min followed by slow cooling to room temperature. EMSA experiments were performed by incubating increasing concentrations of ING5 or the different domains of ING5 with fluorescent DNA ligands at a final concentration of 0.1 µM in a 15-µl reaction mixture containing 20 mM Tris–HCl (pH 8.0), 5 mM $MgCl_2$, 50 mM NaCl, 2 mM DTT, and 0.1 g/L BSA. After incubation for 10 min at room temperature, glycerol was added to 5% (v/v) and the reaction products were separated on a 6% native polyacrylamide gel run at room temperature in cold 0.5× Tris–Borate–EDTA buffer for 50 min at 80 V. Labeled nucleic acid fragments were detected by fluorescence imaging (ImageQuant LAS4000; GE Healthcare), and quantification of protein–nucleic acid complexes was performed with ImageQuant TL image analysis software (GE Healthcare).

Acknowledgments

We thank Pietro Roversi for his help solving the crystal structure of ING5 Nt and for his critical reading of the manuscript, and Tammo Diercks for help with the NMR experiments. This work was supported by grant CTQ2017-83810-R (MINECO/FEDER/UE) to F.J.B., SAF2015-65690P to I.P., SAF2017-84092-R and SAF2014-51966-R to R.K., and SAF2017-84934-R to M.V. G.O. acknowledges a Formación de Personal Investigador Fellowship from MINECO (BES-2012-052851). We also thank

MINECO for the Severo Ochoa Excellence Accreditation (SEV-2016-0644).

Appendix A. Supplementary data

Supplementary data to this article can be found online at https://doi.org/10.1016/j.jmb.2019.04.018.

Received 7 February 2019;
Received in revised form 10 April 2019;
Accepted 10 April 2019
Available online 24 April 2019

Keywords:
ING5;
chromatin;
NMR;
crystallography;
SAXSG.O. and J.A.R. contributed equally to this work.

Abbreviations used:
ING, inhibitor of growth; HSQC, heteronuclear single quantum coherence spectroscopy; CD, circular dichroism; SAXS, small-angle x-ray scattering; Nt, N-terminal domain; NLS, nuclear localization signal; PHD, plant homeodomain; TROSY, transverse optimized spectroscopy; PRE, paramagnetic relaxation enhancement.

References

[1] P.Y. Kan, T.L. Caterino, J.J. Hayes, The H4 tail domain participates in intra- and internucleosome interactions with protein and DNA during folding and oligomerization of nucleosome arrays, Mol. Cell. Biol. 29 (2009) 538–546.
[2] A. Groth, W. Rocha, A. Verreault, G. Almouzni, Chromatin challenges during DNA replication and repair, Cell. 128 (2007) 721–733.
[3] B. Li, M. Carey, J.L. Workman, The role of chromatin during transcription, Cell. 128 (2007) 707–719.
[4] S.D. Taverna, H. Li, A.J. Ruthenburg, C.D. Allis, D.J. Patel, How chromatin-binding modules interpret histone modifications: lessons from professional pocket pickers, Nat. Struct. Mol. Biol. 14 (2007) 1025–1040.
[5] G.H. He, C.C. Helbing, M.J. Wagner, C.W. Sensen, K. Riabowol, Phylogenetic analysis of the ING family of PHD finger proteins, Mol. Biol. Evol. 22 (2005) 104–116.
[6] G. Tallen, K. Riabowol, Keep-ING balance: tumor suppression by epigenetic regulation, FEBS Lett. 588 (2014) 2728–2742.
[7] J.D. Thompson, D.G. Higgins, T.J. Gibson, CLUSTAL W: improving the sensitivity of progressive multiple sequence alignment through sequence weighting, position-specific gap penalties and weight matrix choice, Nucleic Acids Res. 22 (1994) 4673–4680.
[8] M. Russell, P. Berardi, W. Gong, K. Riabowol, Grow-ING, Age-ING and Die-ING: ING proteins link cancer, senescence and apoptosis, Exp. Cell Res. 312 (2006) 951–961.
[9] X. Shi, T. Hong, K.L. Walter, M. Ewalt, E. Michishita, T. Hung, et al., ING2 PHD domain links histone H3 lysine 4 methylation to active gene repression, Nature. 442 (2006) 96–99.
[10] Y. Doyon, C. Cayrou, M. Ullah, A.J. Landry, V. Cote, W. Selleck, et al., ING tumor suppressor proteins are critical regulators of chromatin acetylation required for genome expression and perpetuation, Mol. Cell 21 (2006) 51–64.
[11] P.V. Peña, R.A. Hom, T. Hung, H. Lin, A.J. Kuo, R.P. Wong, et al., Histone H3K4me3 binding is required for the DNA repair and apoptotic activities of ING1 tumor suppressor, J. Mol. Biol. 380 (2008) 303–312.
[12] P.V. Peña, F. Davrazou, X. Shi, K.L. Walter, V.V. Verkhusha, O. Gozani, et al., Molecular mechanism of histone H3K4me3 recognition by plant homeodomain of ING2, Nature. 442 (2006) 100–103.
[13] A. Palacios, I.G. Munoz, D. Pantoja-Uceda, M.J. Marcaida, D. Torres, J.M. Martin-Garcia, et al., Molecular basis of histone H3K4me3 recognition by ING4, J. Biol. Chem. 283 (2008) 15956–15964.
[14] K.S. Champagne, N. Saksouk, P.V. Pena, K. Johnson, M. Ullah, X.J. Yang, et al., The crystal structure of the ING5 PHD finger in complex with an H3K4me3 histone peptide, Proteins. 72 (2008) 1371–1376.
[15] A. Palacios, A. Moreno, B.L. Oliveira, T. Rivera, J. Prieto, P. Garcia, et al., The dimeric structure and the bivalent recognition of H3K4me3 by the tumor suppressor ING4 suggests a mechanism for enhanced targeting of the HBO1 complex to chromatin, J. Mol. Biol. 396 (2010) 1117–1127.
[16] S. Culurgioni, I.G. Munoz, A. Moreno, A. Palacios, M. Villate, I. Palmero, et al., The crystal structure of the inhibitor of growth 4 (ING4) dimerization domain reveals the functional organization of the ING family of chromatin binding proteins, J. Biol. Chem. 287 (2012) 10876–10884.
[17] T. Hung, O. Binda, K.S. Champagne, A.J. Kuo, K. Johnson, H.Y. Chang, et al., ING4 mediates crosstalk between histone H3 K4 trimethylation and H3 acetylation to attenuate cellular transformation, Mol. Cell 33 (2009) 248–256.
[18] A.C. Joerger, S. Rajagopalan, E. Natan, D.B. Veprintsev, C. V. Robinson, A.R. Fersht, Structural evolution of p53, p63, and p73: implication for heterotetramer formation, Proc. Natl. Acad. Sci. U. S. A. 106 (2009) 17705–17710.
[19] V.N. Uversky, Size-exclusion chromatography in structural analysis of intrinsically disordered proteins, Methods Mol. Biol. 896 (2012) 179–194.
[20] K. Dutta, A. Alexandrov, H. Huang, S.M. Pascal, pH-induced folding of an apoptotic coiled coil, Protein Sci. 10 (2001) 2531–2540.
[21] J. Walshaw, D.N. Woolfson, Socket: a program for identifying and analysing coiled-coil motifs within protein structures, J. Mol. Biol. 307 (2001) 1427–1450.
[22] L.S. Swapna, K. Srikeerthana, N. Srinivasan, Extent of structural asymmetry in homodimeric proteins: prevalence and relevance, PLoS One 7 (2012), e36688.
[23] P. Redondo, J. Prieto, I.G. Munoz, A. Alibes, F. Stricher, L. Serrano, et al., Molecular basis of xeroderma pigmentosum group C DNA recognition by engineered meganucleases, Nature. 456 (2008) 107–111.
[24] B. Cengiz, E. Gunduz, M. Gunduz, L.B. Beder, R. Tamamura, C. Bagci, et al., Tumor-specific mutation and downregulation of ING5 detected in oral squamous cell carcinoma, Int. J. Cancer 127 (2010) 2088–2094.
[25] J. Schymkowitz, J. Borg, F. Stricher, R. Nys, F. Rousseau, L. Serrano, The FoldX web server: an online force field, Nucleic Acids Res. 33 (2005) W382–W388.

[26] L.A. Marky, K.J. Breslauer, Calculating thermodynamic data for transitions of any molecularity from equilibrium melting curves, Biopolymers. 26 (1987) 1601–1620.
[27] F. Thomas, A.L. Boyle, A.J. Burton, D.N. Woolfson, A set of de novo designed parallel heterodimeric coiled coils with quantified dissociation constants in the micromolar to sub-nanomolar regime, J. Am. Chem. Soc. 135 (2013) 5161–5166.
[28] U. Linzen, R. Lilischkis, R. Pandithage, B. Schilling, A. Ullius, J. Luscher-Firzlaff, et al., ING5 is phosphorylated by CDK2 and controls cell proliferation independently of p53, PLoS One 10 (2015), e0123736.
[29] C. Leibiger, N. Kosyakova, H. Mkrtchyan, M. Glei, V. Trifonov, T. Liehr, First molecular cytogenetic high resolution characterization of the NIH 3T3 cell line by murine multicolor banding, J. Histochem. Cytochem. 61 (2013) 306–312.
[30] G. Ormaza, B. Medagli, A. Ibanez de Opakua, J.A. Rodriguez, N. Merino, M. Villate, et al., The tumor suppressor inhibitor of growth 4 binds double-stranded DNA through its disordered central region, FEBS Lett. 591 (2017) 425–432.
[31] J.M. Pagano, C.C. Clingman, S.P. Ryder, Quantitative approaches to monitor protein–nucleic acid interactions using fluorescent probes, RNA. 17 (2011) 14–20.
[32] W.P. Jencks, On the attribution and additivity of binding energies, Proc. Natl. Acad. Sci. U. S. A. 78 (1981) 4046–4050.
[33] A.J. Ruthenburg, W. Wang, D.M. Graybosch, H. Li, C.D. Allis, D.J. Patel, et al., Histone H3 recognition and presentation by the WDR5 module of the MLL1 complex, Nat. Struct. Mol. Biol. 13 (2006) 704–712.
[34] G.D. Amoutzias, D.L. Robertson, Y. Van de Peer, S.G. Oliver, Choose your partners: dimerization in eukaryotic transcription factors, Trends Biochem. Sci. 33 (2008) 220–229.
[35] F. Wang, A.Y. Wang, C. Chesnelong, Y. Yang, A. Nabbi, S. Thalappilly, et al., ING5 activity in self-renewal of glioblastoma stem cells via calcium and follicle stimulating hormone pathways, Oncogene. 37 (2018) 286–301.
[36] H.C. Zheng, P. Xia, X.Y. Xu, H. Takahashi, Y. Takano, The nuclear to cytoplasmic shift of ING5 protein during colorectal carcinogenesis with their distinct links to pathologic behaviors of carcinomas, Hum. Pathol. 42 (2011) 424–433.
[37] X. Li, T. Nishida, A. Noguchi, Y. Zheng, H. Takahashi, X. Yang, et al., Decreased nuclear expression and increased cytoplasmic expression of ING5 may be linked to tumorigenesis and progression in human head and neck squamous cell carcinoma, J. Cancer Res. Clin. Oncol. 136 (2010) 1573–1583.
[38] Y.N. Xing, X. Yang, X.Y. Xu, Y. Zheng, H.M. Xu, Y. Takano, et al., The altered expression of ING5 protein is involved in gastric carcinogenesis and subsequent progression, Hum. Pathol. 42 (2011) 25–35.
[39] X.Q. Ding, S. Zhao, L. Yang, X. Zhao, G.F. Zhao, S.P. Zhao, et al., The nucleocytoplasmic translocation and up-regulation of ING5 protein in breast cancer: a potential target for gene therapy, Oncotarget. 8 (2017) 81953–81966.
[40] G. Roscigno, I. Puoti, I. Giordano, E. Donnarumma, V. Russo, A. Affinito, et al., MiR-24 induces chemotherapy resistance and hypoxic advantage in breast cancer, Oncotarget. 8 (2017) 19507–19521.
[41] Q.Y. Zhao, F. Ju, Z.H. Wang, X.Z. Ma, H. Zhao, ING5 inhibits epithelial–mesenchymal transition in breast cancer by suppressing PI3K/Akt pathway, Int. J. Clin. Exp. Med. 8 (2015) 15498–15505.
[42] V.V. Rogov, A. Rozenknop, N.Y. Rogova, F. Lohr, S. Tikole, V. Jaravine, et al., A universal expression tag for structural and functional studies of proteins, Chembiochem. 13 (2012) 959–963.
[43] F.W. Studier, Protein production by auto-induction in high density shaking cultures, Protein Expr. Purif. 41 (2005) 207–234.
[44] R.C. Tyler, H.K. Sreenath, S. Singh, D.J. Aceti, C.A. Bingman, J.L. Markley, et al., Auto-induction medium for the production of [U-15N]- and [U-13C, U-15N]-labeled proteins for NMR screening and structure determination, Protein Expr. Purif. 40 (2005) 268–278.
[45] J. Marley, M. Lu, C. Bracken, A method for efficient isotopic labeling of recombinant proteins, J. Biomol. NMR 20 (2001) 71–75.
[46] R. Sanchez, D. Torres, J. Prieto, F.J. Blanco, R. Campos-Olivas, Backbone assignment of human proliferating cell nuclear antigen, Biomol. NMR Assign. 1 (2007) 245–247.
[47] E. Gasteiger, A. Gattiker, C. Hoogland, I. Ivanyi, R.D. Appel, A. Bairoch, ExPASy: the proteomics server for in-depth protein knowledge and analysis, Nucleic Acids Res. 31 (2003) 3784–3788.
[48] P. Pernot, A. Round, R. Barrett, A. De Maria Antolinos, A. Gobbo, E. Gordon, et al., Upgraded ESRF BM29 beamline for SAXS on macromolecules in solution, J. Synchrotron Radiat. 20 (2013) 660–664.
[49] M.V. Petoukhov, P.V. Konarev, A.G. Kikhney, D.I. Svergun, ATSAS 2.1—towards automated and web-supported small-angle scattering data analysis, J. Appl. Crystallogr. 40 (2007) s223-s8.
[50] P.V. Konarev, V.V. Volkov, A.V. Sokolova, M.H.J. Koch, D.I. Svergun, PRIMUS: a Windows PC-based system for small-angle scattering data analysis, J. Appl. Crystallogr. 36 (2003) 1277–1282.
[51] D.I. Svergun, Determination of the regularization parameter in indirect-transform methods using perceptual criteria, J. Appl. Crystallogr. 25 (1992) 495–503.
[52] D.I. Svergun, M.V. Petoukhov, M.H. Koch, Determination of domain structure of proteins from X-ray solution scattering, Biophys. J. 80 (2001) 2946–2953.
[53] V.V. Volkov, D.I. Svergun, Uniqueness of ab-initio shape determination in small-angle scattering, J. Appl. Crystallogr. 36 (2003) 860–864.
[54] D.I. Svergun, C. Barberato, M.H.J. Koch, CRYSOL: a program to evaluate x-ray solution scattering of biological macromolecules from atomic coordinates, J. Appl. Crystallogr. 28 (1995) 768–773.
[55] M.B. Kozin, D.I. Svergun, Automated matching of high- and low-resolution structural models, J. Appl. Crystallogr. 34 (2001) 33–41.
[56] E.F. Pettersen, T.D. Goddard, C.C. Huang, G.S. Couch, D.M. Greenblatt, E.C. Meng, et al., UCSF Chimera—a visualization system for exploratory research and analysis, J. Comput. Chem. 25 (2004) 1605–1612.
[57] K. Kazimierczuk, V.Y. Orekhov, Accelerated NMR spectroscopy by using compressed sensing, Angew. Chem. Int. Ed. Engl. 50 (2011) 5556–5559.
[58] D.S. Wishart, C.G. Bigam, J. Yao, F. Abildgaard, H.J. Dyson, E. Oldfield, et al., 1H, 13C and 15N chemical shift referencing in biomolecular NMR, J. Biomol. NMR 6 (1995) 135–140.
[59] Y.S. Jung, M. Zweckstetter, Mars—robust automatic backbone assignment of proteins, J. Biomol. NMR 30 (2004) 11–23.
[60] A. Palacios, P. Garcia, D. Padro, E. Lopez-Hernandez, I. Martin, F.J. Blanco, Solution structure and NMR characterization of the binding to methylated histone tails of the plant

homeodomain finger of the tumour suppressor ING4, FEBS Lett. 580 (2006) 6903–6908.
[61] M.G. Bomar, M.T. Pai, S.R. Tzeng, S.S. Li, P. Zhou, Structure of the ubiquitin-binding zinc finger domain of human DNA Y-polymerase eta, EMBO Rep. 8 (2007) 247–251.
[62] Z. Otwinowski, W. Minor, Charles W. Carter Jr., Processing of X-ray Diffraction Data Collected in Oscillation Mode. Methods in Enzymology, Academic Press, 1997 307–326.
[63] A.J. McCoy, R.W. Grosse-Kunstleve, P.D. Adams, M.D. Winn, L.C. Storoni, R.J. Read, Phaser crystallographic software, J. Appl. Crystallogr. 40 (2007) 658–674.
[64] N. Stein, CHAINSAW: a program for mutating pdb files used as templates in molecular replacement, J. Appl. Crystallogr. 41 (3) (2008).
[65] P. Emsley, K. Cowtan, Coot: model-building tools for molecular graphics, Acta Crystallogr. D Biol. Crystallogr. 60 (2004) 2126–2132.
[66] M.D. Winn, C.C. Ballard, K.D. Cowtan, E.J. Dodson, P. Emsley, P.R. Evans, et al., Overview of the CCP4 suite and current developments, Acta Crystallogr. D Biol. Crystallogr. 67 (2011) 235–242.
[67] K. Cowtan, The Buccaneer software for automated model building. 1. Tracing protein chains, Acta Crystallogr. D Biol. Crystallogr. 62 (2006) 1002–1011.
[68] E. Blanc, P. Roversi, C. Vonrhein, C. Flensburg, S.M. Lea, G. Bricogne, Refinement of severely incomplete structures with maximum likelihood in BUSTER-TNT, Acta Crystallogr. D Biol. Crystallogr. 60 (2004) 2210–2221.
[69] H.R. Powell, The Rossmann Fourier autoindexing algorithm in MOSFLM, Acta Crystallogr. D Biol. Crystallogr. 55 (1999) 1690–1695.
[70] P. Evans, Scaling and assessment of data quality, Acta Crystallogr. D Biol. Crystallogr. 62 (2006) 10.
[71] A. Vagin, A. Teplyakov, Molecular replacement with MOLREP, Acta Crystallogr. D Biol. Crystallogr. 66 (2010) 22–25.
[72] G.N. Murshudov, P. Skubak, A.A. Lebedev, N.S. Pannu, R.A. Steiner, R.A. Nicholls, et al., REFMAC5 for the refinement of macromolecular crystal structures, Acta Crystallogr. D Biol. Crystallogr. 67 (2011) 355–367.
[73] G.N. Ramachandran, C. Ramakrishnan, V. Sasisekharan, Stereochemistry of polypeptide chain configurations, J. Mol. Biol. 7 (1963) 95–99.
[74] V.B. Chen, W.B. Arendall 3rd, J.J. Headd, D.A. Keedy, R.M. Immormino, G.J. Kapral, et al., MolProbity: all-atom structure validation for macromolecular crystallography, Acta Crystallogr. D Biol. Crystallogr. 66 (2010) 12–21.
[75] E. Krissinel, K. Henrick, Inference of macromolecular assemblies from crystalline state, J. Mol. Biol. 372 (2007) 774–797.
[76] Schrödinger. The PyMOL Molecular Graphics System, Version 1.5.0.4 Schrödinger, LLC. In: 1.5.0.4, editor. 1504 1.5.0.4 ed2010.
[77] N. Bengoa-Vergniory, I. Gorrono-Etxebarria, I. Gonzalez-Salazar, R.M. Kypta, A switch from canonical to noncanonical Wnt signaling mediates early differentiation of human neural stem cells, Stem Cells 32 (2014) 3196–3208.
[78] N. Avvakumov, M.E. Lalonde, N. Saksouk, E. Paquet, K.C. Glass, A.J. Landry, Y. Doyon, C. Cayrou, G.A. Robitaille, D. E. Richard, X.J. Yang, T.G. Kutateladze, J. Côté, Conserved molecular interactions within the HBO1 acetyltransferase complexes regulate cell proliferation, Mol. Cell Biol. 32 (3) (2012 Feb) 689–703, https://doi.org/10.1128/MCB.06455-11.